TITLE:

Observations of Cosmic TeV γ-rays in the Southern Sky by Means of Stereoscopic and Timing Analyses of Cherenkov Light

AUTHOR(S):

Susukita, Ryutaro

CITATION:

Susukita, Ryutaro. Observations of Cosmic TeV γ-rays in the Southern Sky by Means of Stereoscopic and Timing Analyses of Cherenkov Light. Memoirs of the Faculty of Science, Kyoto University. Series of physics, astrophysics, geophysics and chemis ...

ISSUE DATE:

1998-03

URL:

http://hdl.handle.net/2433/257646

RIGHT:

京都大学学術情報リポジトリ
KURENAI 紅
Kyoto University Research Information Repository

Memoirs of the Faculty of Science, Kyoto University, Series of Physics, Astrophysics, Geophysics and Chemistry, Vol. XXXX, No. 2, Article 1, 1998

Observations of Cosmic TeV γ-rays in the Southern Sky by Means of Stereoscopic and Timing Analyses of Cherenkov Light

By

Ryutaro SUSUKITA*

Department of Physics, Faculty of science, Kyoto University
Kyoto 606-8502, Japan

(Received Feburuary 28, 1997)

Abstract

A search for TeV γ-rays from the pulsars PSR B1706−44 and PSR B1055−52 and from the radio galaxy Centaurus A were made as a project of the CANGAROO collaboration with two atmospheric Cherenkov telescopes, the 3.8 m telescope and the BIGRAT, at Woomera, Australia in 1994 and 1995. The times of observations were 27 hours, 69 hours and 57 hours, respectively. Stereoscopic analysis and timing analysis in addition to the imaging technique have been applied to the observational data. Two images of Cherenkov light from one shower detected with the two telescopes equipped with different resolution cameras have been utilized in the stereoscopic analysis. In the timing analysis the arrival direction of the shower has been determined from the fact that the arrival time of a Cherenkov photon on the detector depends upon the direction of the photon. The improvement of S/N by using the stereoscopic analysis and timing analysis has been shown in the case of observational data of PSR B1706−44. The S/N of 0.16 obtained by the imaging technique has been improved to 0.91 by using the stereoscopic and timing analyses. This improvement reduces the necessary time for observation by a factor of 4.

TeV γ-rays from PSR B1706−44 have been detected. The significance is 4.9 σ. The flux above the energy has been found to be $(1.3\pm0.4)\times10^{-11}\left(\frac{E}{\mathrm{TeV}}\right)^{-1.9}\mathrm{cm}^{-2}\mathrm{s}^{-1}$ if the power-law index is assumed to be -2.9. The energy threshold of the observation is approximately 2 TeV. This flux is consistent with the one which was observed in 1992-1993. From the observations in 1992-1995, it has been confirmed that PSR B1706−44 is a stable TeV γ-ray emitter. There is no evidence for TeV γ-rays from PSR B1055−52. The upper limit of the flux above 2 TeV was $9.5\times10^{-13}\mathrm{cm}^{-2}\mathrm{s}^{-1}$. It is expected that there is a break in the spectrum between 4 GeV and 2 TeV. There is no evidence also for TeV γ-rays from Centaurus A. The upper limit of the flux above 2 TeV was $1.5\times10^{-12}\mathrm{cm}^{-2}\mathrm{s}^{-1}$.

1. Introduction

1.1. TeV γ-ray astronomy

Cosmic TeV γ-rays are closely related to high energy phenomena in the universe such as the acceleration mechanism of charged particles of cosmic rays.

*Present address: The Institute of Physical and Chemical Research, Wako 351-01, Japan

Although only a short time has passed after the observation of the first convincing signals from point sources, the TeV γ-ray astronomy has become an important field mainly because of the recent improvement of the detector sensitivity. Signals of TeV γ-rays were confirmed with high enough significance, which is larger than 20 σ[1] [2]. Following this result, the number of confirmed TeV γ-ray sources is increasing. Further searches have been stimulated by the discovery of γ-ray sources at the energy of 20 MeV to 30 GeV with the EGRET detector of CGRO (Compton Gamma Ray Observatory) satellite launched in 1991.

TeV γ-ray sources may include several types of celestial bodies, that is, radio pulsars, supernova remnants (SNRs), active galactic nuclei (AGNs), X-ray binaries, cataclysmic variables etc. Radio pulsars, SNRs and AGNs are discussed in this dissertation.

Pulsars and SNRs, which are closely related to each other, are candidates for TeV γ-ray sources. The angular resolutions of current TeV γ-ray detectors are poorer than those used for longer wavelength such as the ones of the radio astronomy. Therefore, it is difficult to distinguish the emissions from the two closely located objects even in the case that they are resolved from each other in the radio or X-ray astronomy etc. TeV γ-rays from the Crab pulsar or nebula have been observed by the Whipple collaboration. The CANGAROO (Collaboration of Australia and Nippon for GAmma Ray Observatory in the Outback) group has observed the emission of TeV γ-rays from PSR B1706−44. The CANGAROO group has confirmed TeV γ-rays from the Crab[4] and has recently also observed TeV γ-rays from the direction of the Vela pulsar[5]. There appear no pulsed components in the γ-rays from these sources. The pulsed emission with the same period as that of the radio pulsar should be strong evidence for the fact that TeV γ-rays are emitted from the pulsar magnetosphere. Although several observations of the pulsed γ-rays from various pulsars including the Crab pulsar have been reported, none of them have been confirmed by other groups.

The energy spectrum of the γ-rays from the Crab in TeV region appears to follow the power law with differential exponent of roughly -2.7 in the energy range of 0.5 TeV to 10 TeV. No time variation of the flux from the Crab has been found.

There are several models which have been proposed to explain γ-ray emission up to GeV energies from the pulsar magnetosphere, but these models have uncertainties in concluding if the γ-ray emission extends to the energy region of TeV. As for the Crab nebula, the synchrotron the self-Compton model by de Jager and Harding explains the features of the observed unpulsed emission of the γ-rays from the Crab in the energy region between 100 MeV and 10 TeV[6]. In this model TeV γ-rays result from inverse Compton scattering of low energy photons by relativistic electrons which are accelerated by shock wave at the interface between plasma flow from the pulsar and the nebula surrounding the pulsar. In the case of self-Compton model, intense synchrotron radiation in the Crab nebula provide with target photons for the inverse Compton process. However, PSR B1706−44 has no apparent nebula and the microwave background of 2.7 K presumably serves as the

target photons. SNRs are generally believed to the most likely origin of cosmic rays in the energy region below 10^{14}eV. Charged particles should be accelerated by shock waves on the SNR surface. It is expected that γ-rays are produced in π^0 decay originated in hadron-hadron collisions in SNRs. Thus, TeV γ-rays from SNRs would give strong indication for acceleration of cosmic rays.

Two AGNs, Markarian 421 ($z=0.031$) [7] and Markarian 501 ($z=0.033$) [8], have been also reported to be TeV γ-ray emitters. The ray flux from Mrk 421 shows a violent time-variable feature as in the case of X-rays. In the energy region of 100 MeV to 10 GeV, about 40 AGNs which emit γ-rays are found. Most of them belong to the blazar class. These AGNs are considered to emit γ-rays in the directions of the relativistic jets with which the blazars are accompanied. Models proposed for explanation of the origins of γ-rays from AGNs can be classified into leptonic models and hadronic models. In the former models γ-rays are produced in inverse Compton scattering of low energy photons by relativistic electrons in the jet. In the latter ones the origin of γ-rays is in decay of pions produced in hadron-hadron interactions in the jet. The answer is still controversial. Observations of energy spectra above 10 GeV may provide with a clue to infer that either of the models is more likely the case.

In the case of extragalactic sources it is necessary to take account of the absorption of TeV γ-rays in the intergalactic space [9]. The dominant absorption process is

$$\gamma+\gamma(\text{infrared}) \rightarrow e^+ + e^-.$$

The attenuation of TeV γ-rays increases with the distance from the earth to the source, and gives information of the infrared intensity in extragalactic space, which is useful to know the past activity of galaxies. Since the observation of the infrared radiation in the intergalactic space is difficult, the precise evaluation of the effect has not been done. Although numerous AGNs which emit γ-rays in the energy region of 100 MeV to 10 GeV have been discovered, no convincing evidence for emission of TeV γ-rays from AGNs has been found except those from the two sources [10]. The two sources are BL Lac objects very close to the earth. It is important to know whether the inferred break of the energy spectrum between the energy region of 100 MeV to 10 GeV and TeV is caused by the attenuation effect or by the cutoff of acceleration of progenitor particles.

In addition to the objects from which a search for TeV γ-rays was stimulated by the results in the energy region of GeV, Cygnus X-3, Hercules X-3, Vela X-1 and a cataclysmic variable AE Aquarii have been reported as sources of TeV γ-rays, although they have not been confirmed [11] [12]. The emission of TeV γ-rays from these objects is, a remarkable implication in high energy astrophysics because no γ-rays have been seen in the energy region of MeV to GeV.

1.2. Observed sources

This dissertation reports on three objects, PSR B1706−44, PSR B1055−52 and Centaurus A (Cen A). The observations were carried out at Woomera in South

Australia using the telescopes of the CANGAROO group in 1994 and 1995. CANGAROO is a project to observe TeV γ-rays using two imaging atmospheric Cherenkov telescopes. In addition to the sources mentioned above, the binary pulsar PSR B1259−63, the SNR W28, the AGNs PKS 0521−365 and PKS 2005−489 etc. were observed using the telescopes.

1.2.1. Pulsars

PSR B1706−44 is a young pulsar with a period of 102 ms, located at about 1.5 kpc. The characteristic age is 1.7×10^4 years. TeV γ-rays from this object were observed in 1992 and 1993 by the CANGAROO group for the first time using a Cherenkov-light telescope[3]. The flux was $(1.1 \pm 0.2) \times 10^{-11}\mathrm{cm}^{-2}\mathrm{s}^{-1}$ in the energy region above 1 ± 0.2 TeV.

The major part of the emitted γ-rays is likely unpulsed. The upper limit of the γ-ray flux was reported to be $5.8 \times 10^{-12}\mathrm{cm}^{-2-1}$ above 2.6 TeV for the pulsed component[13]. Observations of the source in the following years, which are described in this dissertation, are important to confirm the previous detection of TeV γ-rays and to inspect the stability of the flux. The observation time spent on the source is shorter in 1994 and 1995 than in 1992 and 1993, resulting in a poor statistics. However, we attempt to apply new methods for studying γ-ray-emitting objects and to improve detection sensitivity.

PSR B1055−52 is one of the seven known γ-ray pulsars in the energy region of MeV to GeV. The distance from the earth has been estimated to be 1.5 kpc. It was discovered as a radio pulsar with a period of 197 ms[14]. The characteristic age is 5.3×10^5 years. It is the oldest of the known γ-ray pulsars detected by EGRET. Pulsed emission in the energy region of 100 MeV to 4 GeV has been observed using EGRET aboard the Compton Gamma Ray Observatory[15]. The power-law index of the energy spectrum in this energy region is -1.18 ± 0.16. The spectrum is the hardest among all the observed γ-ray pulsars. No unpulsed γ-rays have been detected. The ratio of the γ-ray luminosity between 100 MeV and 5 GeV to the rotational energy loss of the pulsar is 0.31. The value is the highest among all the observed γ-ray pulsars. In particular, it is 10^3 times as large as the one from the Crab. If we assume that the hard spectrum extends to energies higher than the EGRET detection, the total luminosity exceeds the rotational energy loss of the pulsar. Therefore, it is natural to presume that the power-law index changes in higher energy region. Observations in TeV region will provide important information on the energy spectrum. Since this pulsar is the oldest γ-ray pulsar among the seven, the observation will contribute to our further understandings on the relation between the age of pulsar and TeV γ-ray emission from pulsars.

1.2.2. Centaurus A

Cen A is a radio galaxy located at about 3.5 Mpc, which is much closer than Mrk 421 and Mrk 501 to the earth. Due to the short distance between the earth and the object attenuation of TeV γ-rays in intergalactic space is negligible. This advantage may allow us to observe the primary γ-ray flux from this AGN in higher energy region than TeV independent of the intergalactic infrared-photon density. A detection of TeV γ-rays from Cen A was reported in 1975[16], however, with no

confirmation by other groups in the following years. In the energy region of MeV to GeV an unidentified γ-ray source has been observed within an error circle including Cen A [17] [18] and a BL Lac object about 2° apart from the direction of Cen A.

Since Cen A is one of the closest AGNs, TeV γ-rays are possibly of detectable flux even if the luminosity is relatively small. The detection of γ-rays in the energy region of MeV to GeV from the direction of Cen A is encouraging for observation of TeV γ-rays. The observation of γ-rays from a radio galaxy, which is quite different from blazers which emit GeV γ-rays, is helpful for an understanding of high energy processes in AGNs, one of the emission mechanism possibly related to the radio lobe rather than to the relativistic jet.

1.3. Technique for TeV γ-ray observation

The method for observing cosmic TeV γ-rays is described below. Primary cosmic γ-rays in TeV region interact with materials in the atmosphere before reaching the ground. Therefore, observations are performed on the ground using mirrors which collect Cherenkov radiation from extensive air showers (EASs) initiated by TeV γ-rays.

1.3.1. Extensive air showers

A TeV γ-ray forms an electromagnetic cascade shower in the atmosphere. The shower consists mainly of $e^{\pm}$ and γ. Charged particles in the shower with velocities greater than the light velocity in the atmosphere emit Cherenkov light. Almost all the radiation is emitted at a small angle ($\leq 1.4°$) to the direction of the

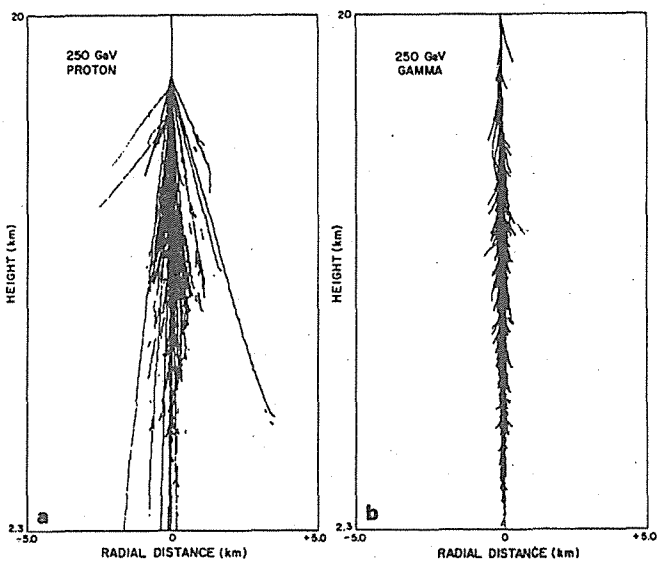

Fig. 1. Simulations for EAS. Side views of particle tracks are shown. The primary particles are (a) a 250 GeV proton and (b) a 250 GeV γ-ray. It indicates that the two EASs are different in angular and lateral distributions of particles.

particle. The directions of the particles are distributed around the directions of the primary γ-rays so that the resultant Cherenkov photons are directional. The photons are distributed in the area with the diameter of about 100 m at sea level in the case of 1 TeV γ-rays if the direction of the primary γ-ray is vertical. It enables us to observe γ-rays with a large collection area. It is possible to discriminate the Cherenkov light from starlight and other light at night using optical devices with good time resolution, since the duration of the Cherenkov light is shorter than 10 ns.

Primary high energy charged particles are also the origins of EASs. They produce mesons and nucleons by interactions with nuclei in the atmosphere. The created π^0's decay into 2γ's, which create electromagnetic showers. The hadron-hadron interactions produce secondary particles with relatively large transverse velocities. The flux of the charged particles is much larger than that of γ-rays in the TeV region. Selection of the EASs initiated by γ-rays is of vital importance in such observations. The average angular and lateral spreads of the particles in EASs initiated by charged particles are large and their angular and lateral distributions are irregular compared with those of γ-ray-initiated EASs (Figure 1). Inheriting these properties, angular and lateral distributions of Cherenkov photons from the hadron-initiated EASs are wider and more irregular than those of γ-ray-initiated EASs. This difference between γ-ray-initiated EASs and hadron-initiated ones is used to identify the primary γ-rays.

1.3.2. Image analysis

Emitted Cherenkov photons from an EAS are collected with a spherical or parabolic reflector in order to detect them with a camera on the focal plane. The angular distribution of Cherenkov photons is detected with the camera. It corresponds to the image of the shower. The image reflects information on the shower, e.g. the arrival direction. The shape of the image is similar to an ellipsoid

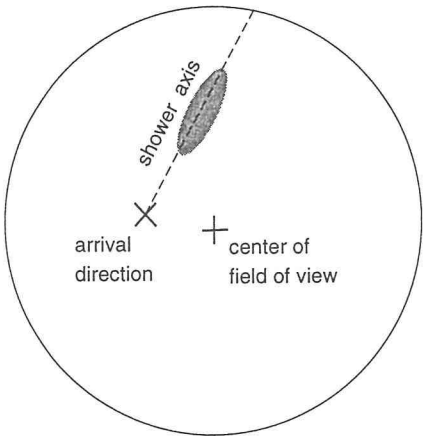

Fig. 2. Image of Cherenkov light from EAS on the focal plane. The shaded ellipsoid indicates the image. It lies along the shower axis, so that it points to the arrival direction of the EAS on the image plane.

whose major axis lies along the shower axis on the image plane (Figure 2). The major axis of the ellipsoid points to the arrival direction of shower on the image plane. It is one of the important characteristics of an image of Cherenkov light from a shower. If the position of the source of γ-rays is point-like on the image plane, the images originated from the γ-rays point to the position. On the other hand, the directions of images originated from background cosmic rays on the image plane are randomly distributed since these cosmic rays are isotropic. Therefore, the γ-rays from the point source are discriminated from background cosmic rays by measuring the orientation of the image. The previous results of the CANGAROO group have been obtained by this image analysis.

However, the previous image analyses are not sufficient to determine the arrival direction of the shower. In order to improve the angular resolution of the arrival direction and S/N, we developed two novel techniques, that is, stereoscopic analysis and timing analysis.

1.3.3. Stereoscopic analysis

It has been pointed out on the basis of Monte Carlo simulations that better angular resolution will be obtained by means of two Cherenkov mirrors located about 100 m apart. This technique, referred as stereoscopic analysis hereafter, has been applied to our observation for the first time*. In this dissertation the results of stereoscopic observation of the γ-rays from PSR B1706−44 using the two detectors of the CANGAROO group are shown. There are two advantages in the stereoscopic analysis. First, the candidates for γ-ray shower obtained with the data of one detector are further selected with the data of the other one. The signal-to-noise ratio of selected showers by using the both detectors should be better than that by using a single detector. Secondly, the difference between the directions toward a shower position from the two detectors can be measured. From such information the position and the direction of the shower can be determined with better accuracy.

1.3.4. Timing analysis

The arrival time of Cherenkov photons reflects the process of the shower development in the atmosphere. It has been suggested that the measurement of the overall timing spectrum of the photons arriving at the Cherenkov mirror is useful to discriminate γ-ray-initiated showers from hadron-initiated ones[21]. In the previous experiments no correlation between the arrival time and the direction of photons has been measured. Therefore, improvement of the signal to noise ratio has been limited. The information of the arrival time for each phototube of the Cherenkov mirror is of importance to find out such a correlation. In particular, we have reconstructed the arrival direction of each shower from the correlation in this

* The development of an EAS has been studied by stereoscopic observations independently at the time when this work has been carried out. One of them is the observation of AEA qr[19]. It has been argued that the approach provides better signal-to-noise ratio for TeV γ-rays due to the different behavior in the development of γ-rays from that in the case of hadrons. It has been also reported that the angular resolution for γ-rays is improved by the stereoscopic observation of the Crab with the HEGRA telescopes[20].

work. It results in better angular resolution than that when the information of arrival time is not available.

We obtained higher sensitivity to TeV γ-rays than that of previous measurements by employing the stereoscopic and the timing analyses for data observed with the CANGAROO telescopes. As a result, emission models of TeV γ-rays from pulsars, SNRs and AGNs are more strongly constrained. The features of the two CANGAROO telescopes, that is, the 3.8-m telescope and the BIGRAT, and the observation procedures including stereoscopic observation are described in Section 2. The procedures for the stereoscopic and timing analyses in addition to the image analysis of obtained data are given in Section 3. The improvement of S/N by the stereoscopic and timing analyses and the the calculated fluxes of the sources noted above are shown in Section 4. The results are discussed in Section 5. The work in the dissertation is concluded in Section 6.

2. Observation

The observing site is located at Woomera (31°6'S, 136°47'E, 160 m above sea level), South Australia. The site is located in a dry region. Clear skies are expected all the year around. Since the closest town, which is very small one, is located 13 km away from the site, observations do not suffer from artificial light. The two telescopes have been named '3.8-m telescope' and 'BIGRAT' (the BIcentennial Gamma RAy Telescope). The 3.8-m telescope was transferred from Dodaira Observatory where it was used for lunar ranging. The BIGRAT was constructed as a TeV γ-ray telescope in 1988. The two telescopes are located 100 m apart, the 3.8-m telescope being placed east of the BIGRAT.

Observations are usually performed for two weeks around a new moon. The observation begins at the end of astronomical twilight in the evening and ends at the beginning of astronomical twilight in the morning before the moonrise or after the moonset. Observations are not carried out when there is a cloud in the direction toward which the telescopes are pointed.

Emission from a point source is confirmed by the difference between the number of observed events from the direction of the source and that from different directions. The off-source observation is carried out to estimate the number of cosmic-ray background from the direction of the source. The direction of the observation of background cosmic rays is chosen to cover the same elevation and azimuthal angle as in the case of the on-source observation.

Starlight is a background for Cherenkov photons. It is preferable that there are no bright stars in the field of view of the camera in observing runs. The directions to be pointed in off-source runs are usually chosen so that there are no stars brighter than magnitude of five in the field of view.

2.1. 3.8-m telescope

The 3.8-m telescope consists of a parabolic reflector 3.8 m in diameter and a

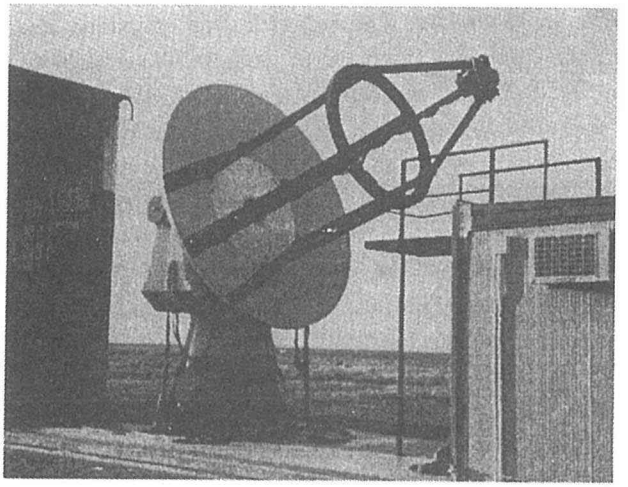

Fig. 3. The 3.8-m telescope. A camera consisting of phototubes is placed at the focal plane of a parabolic reflector 3.8 m in diameter. The focal length is 3.8 m.

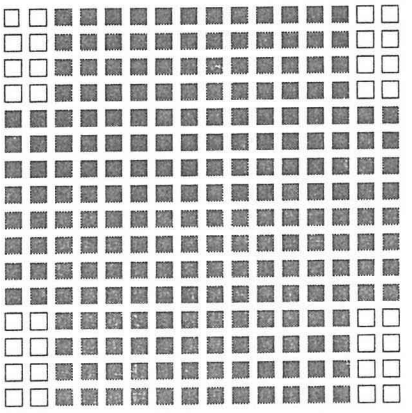

Fig. 4. The layout of phototubes in the camera of the 3.8-m telescope. The number of the tubes (solid squares) was 220 until April, 1995. Then, 32 phototubes (white square) have been added at the edges in order to extend the field of view. The squares represent 10 mm × 10 mm phototubes. The size of whole of the camera is 192 mm × 192 mm square.

high resolution camera at the focal plane on an mount which is rotated around the horizontal axis and the vertical one (altitude-azimuth mount). A photograph of the telescope is shown in Figure 3. The reflector was originally used to measure the distance between the earth and the moon at Dodaira Observatory. The focal length of the reflector is 3.8 m. The central region of the reflector consists of a duralumin mirror 1.7 m in diameter. The outer region consists of six aluminum mirrors. The angular size of the image on the focal plane for light which is parallel to the axis of the reflector is smaller than 0.01°. The reflectivity of the reflector was about 80% when it was manufactured. The current value is about 50%. The path lengths of incident light are the same for the all the position of reflection in the case that the directions of the light are the same as the axis of the mirror. The fact enables us to measure the precise arrival time of each Cherenkov light with the camera placed at the focal plane of the telescope. The tracking accuracy of the mirror is 0.01°.

The camera on the focal plane consisted of 220 phototubes (Hamamatsu R2248) until April, 1995. Then 32 phototubes were added at the four edges in order to enlarge the field of view. The tubes are installed as a square array as shown in Figure 4. The aperture of the camera is 2.8°×2.8°. The photocathode of the tube

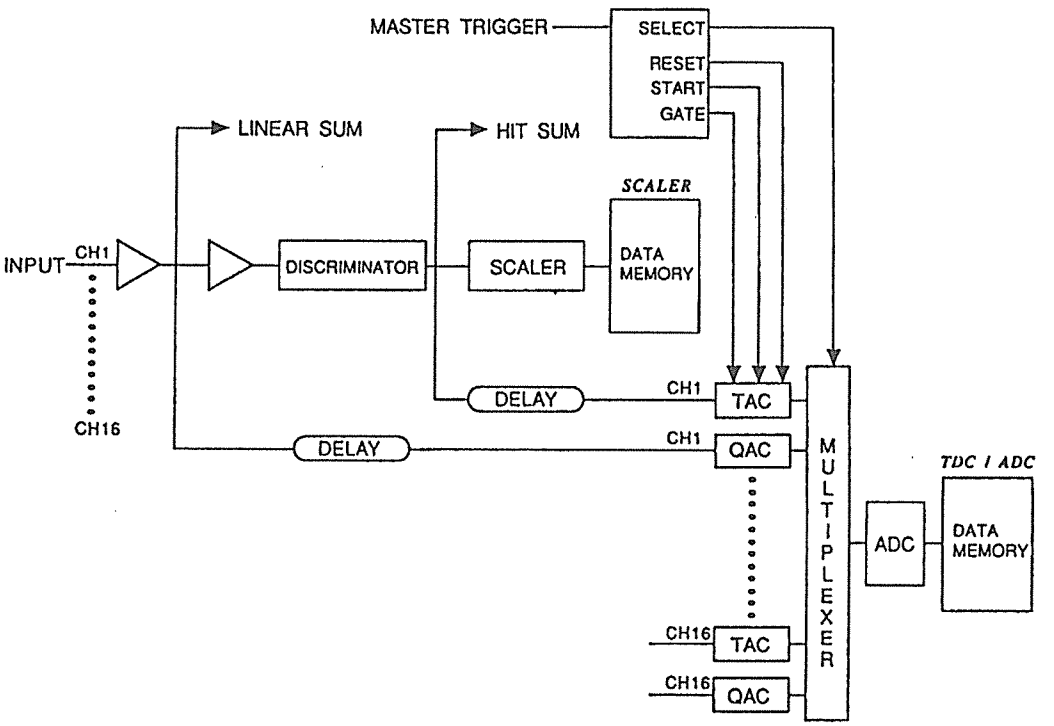

Fig. 5. Cherenkov Circuit Module (CCM). It was designed for processing signals from the phototubes of the 3.8-m telescope. TDCs and ADCs for 16 phototubes are included in one CCM. TACs are Time to Analog Converters. QACs are Charge to Analog Converters.

is made of bialkali. It is sensitive to light of 300 to 650 nm in wavelength. The rise time of the output pulse of the tube is about 0.9 ns. The size of each tube is 10 mm × 10 mm square. The sensitive area is 8 mm × 8 mm. It corresponds to the acceptance of the arrival direction of 0.12° × 0.12°. The space between the tubes is 4 mm, which corresponds to 0.06°. A light-emitting diode (LED) is placed about 50 cm from the front surface of the camera in order to monitor the gains of the tubes and the pedestals of time-to-digital converters (TDCs).

Signals from the tubes are amplified in a module box which is attached to the back of the camera. The signals are amplified in the box in order to reduce the influence of electrical noise on the cable which is roughly 30 m long from the camera to the control room. The coincidence among four signals from the tubes forms a 'hit-sum' signal. The time window is 20 ns. The threshold value of signal pulse height from each tube corresponds to three or four photoelectrons. The 'linear-sum' signal is generated if the summation of pulse height of the signals from all the tubes exceeds a threshold value which corresponds to about 20 photoelectrons. Event-trigger signals are formed in the case of coincidence between the 'hit-sum' signal and the 'linear-sum' signal. The trigger signal opens the gates for analog-to-digital converters (ADCs). The gate width is 50 ns. One photoelectron corresponds to about 20 ADC counts. Counting of the TDCs is started by trigger signals. Delayed signals from the discriminators for tube signals work as stop signals. The time resolution of a TDC is 0.25 ns. The range of TDC counts is

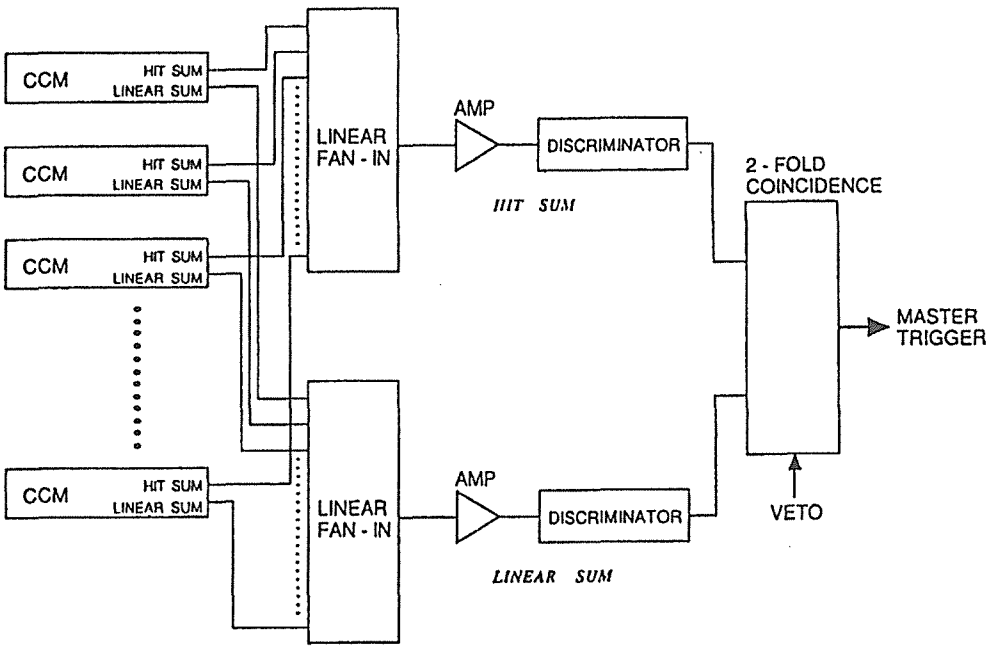

Fig. 6. The block diagram of the system of event trigger generation for the 3.8-m telescope. CCMs (Figure 5) are used to process the signals from phototubes.

Table 1 The periods of observation using the 3.8-m telescope.

Source	Month	Time of observation (hours)
PSR B1706−44	1994 May	9.4
	1995 May-Jul.	17.7
PSR B1055−52	1994 Mar.-Apr.	54.3
	1995 Mar.	14.5
Cen A	1995 Mar.-May	56.5

1 μs. The absolute time of shower arrival is measured to an accuracy of 100 μs using a Global Positioning System (GPS). The absolute times of shower arrivals, ADC counts and TDC counts are recorded on a magnetic tape using a VME on-board computer. The block diagram of data acquisition system is illustrated in Figures 5 and 6.

Most of the triggers of each tube are formed by background photons such as starlight and airglow. The rates vary with the amount of background. A bright star of magnitude 3.3, η Scorpii, is located in the direction of 1.4° from PSR B1706−44. The star is within the field of view of the camera when PSR B1706−44 is tracked. In this case the rate of signals from the tube on which the image of η Scorpii is focused increases to about 1 MHz at the maximum. When PSR B1055−52 and Cen A are observed, there are no bright stars within the field of view. The event rate is about 1 Hz including false events in the observations of all the above objects. The false events are formed by accidental coincidences among the triggers of the tubes when the sky is bright in the field of view. In these cases, the event rates are different between on-source runs and corresponding off-source runs. However most of the false events formed by background photons are eliminated in the off-line analysis.

Usually, prior to each observing run, two types of calibrations are made. The first one is the calibration of ADCs by means of external triggers. The second one is the calibration of tubes and TDCs by means of external triggers coincident with LED flashes. These data are used for calculation of pedestals of ADCs and TDCs as well as calibration of gains of the tubes.

The periods of observations using the 3.8-m telescope described in this dissertation are listed in Table 1.

2.2. BIGRAT

The BIGRAT is constructed of three composite reflectors and a camera on a single altitude-azimuth mount as shown in Figure 7. Each reflector is 4 m in diameter, consisting of 19 mirrors. The mirrors are made of 10 mm-thick glass coated with aluminum. The surface of the central reflector is parabolic with a focal length of 2.7 m. The intensity of light versus the position on the focal plane for a point source at infinity is called the point spread function. The full width at half maximum of the point spread function of the reflector is measured to be 0.35° in the case of the light which is parallel to the axis of the reflector. The surface of the two outer reflectors are parabolic with the same focal lengths. The tracking

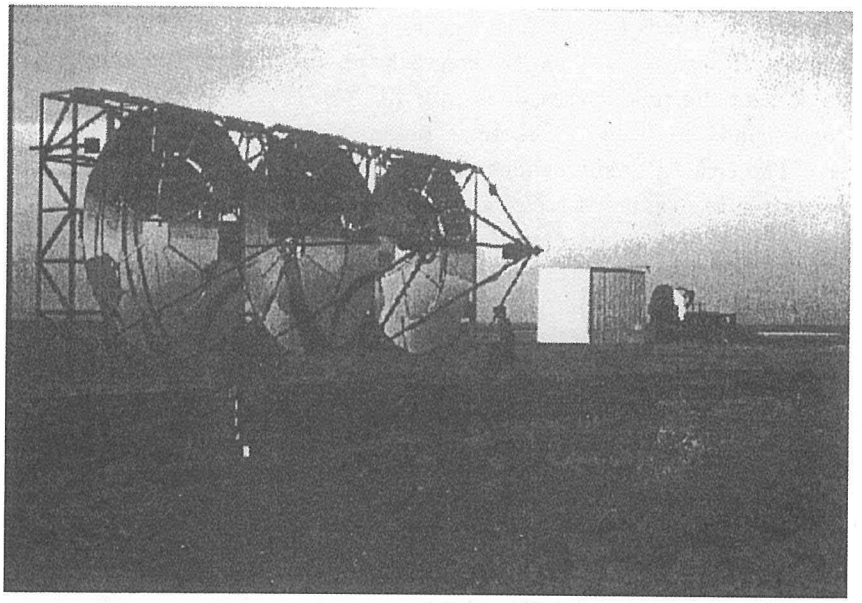

Fig. 7. The BIGRAT. Three reflectors 4 m in diameter are operated single mount. A camera consisting of phototubes is placed at the focal plane of the central reflector. Phototubes are placed at the focal planes of outer reflectors. The focal length of each reflector is 2.7 m.

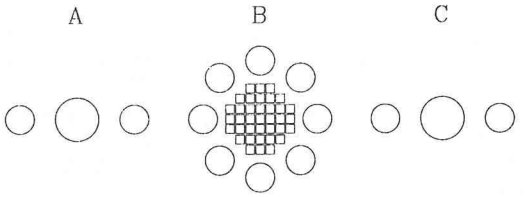

Fig. 8. The layout of phototubes of the BIGRAT. A and C are the detectors for the outer reflectors and B is the camera for the central reflector. The large and small circles represent three- and two-inch tubes respectively. The squares represent 12 mm × 12 mm tubes.

Table 2 Characteristics of the 3.8-m telescope and the BIGRAT.

	3.8-m telescope	BIGRAT
Reflector size	3.8 m in diameter	4 m in diameter × 3
Number of phototubes in camera	220 (256)*	37
Field of view	2.8° × 2.8°	2.3° in diamerter
Timing of output of phototube	measured	not measured
Energy threshold for γ-rays	~1 TeV	~0.4 TeV

*Phototubes were added to the camera of the 3.8-m telescop in April, 1995.

accuracy of the mirror is 0.09°. The camera for the central reflector is an array of 37 phototubes (Figure 2.2). The size of each tube is 12 mm × 12 mm square. The sensitive area of the tube corresponds to 0.21° × 0.21°. The spacing between the tubes corresponds to 0.14°. The total field of view of the camera is 2.3° in diameter. The camera is surrounded with eight tubes of two inches installed on a circumference. The radius of the circle corresponds to 2.2°. These tubes are used for monitoring sky conditions during the observation. The detector for each outer reflector is constituted of a three-inch phototube on axis and two two-inch ones whose centers are 2.2° apart from the three-inch tube. The two-inch tubes are used to monitor the sky conditions. LEDs are placed about 1 m front of the camera in order to monitor the gains of the tubes. The tubes of the camera were equipped with padding lamps consisting of LEDs after observations for PSR B1706−44 in 1994. Background photons are artificially increased when the lamps are turned on. The lamps are used to maintain a constant level of background photons.

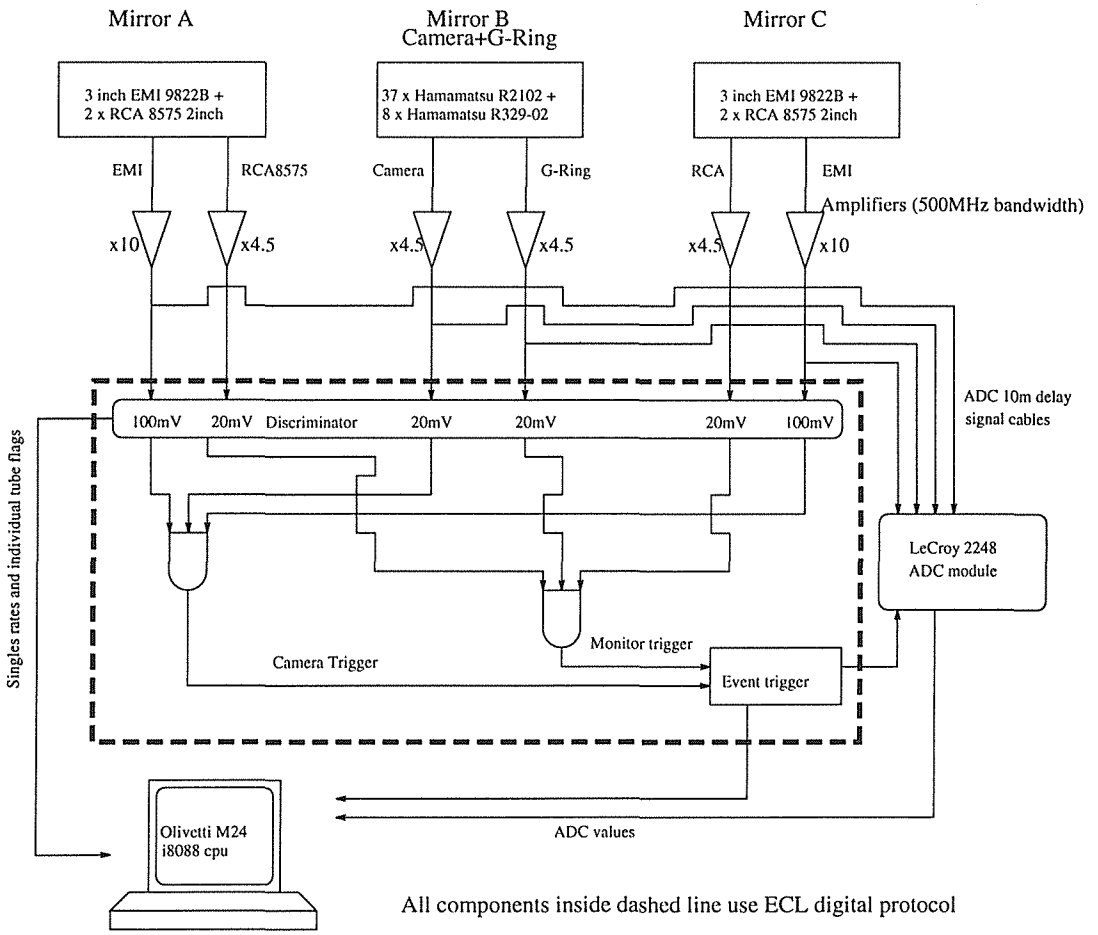

Fig. 9. The block diagram of the data acquisition system of the BIGRAT.

The signals from the tubes are sent to discriminators and ADCs. The outputs of the discriminators from the camera tubes are used to form "event triggers". The threshold value of the signal pulse height from each tube of the camera corresponds to 6 photoelectrons. Those for the two three-inch tubes are estimated to be 46 and 28 photoelectrons. One photoelectron corresponds to approximately 2 ADC counts in the case of the camera tubes. Event-trigger signals are formed in the case of the coincidence between any one of the inner 30 camera tubes and both three-inch tubes. The time window is about 8 ns. The trigger pulse leads to the ADC gates. The gate time is 15 ns. The absolute arrival time is measured to an accuracy of 100 μs with a rubidium clock which is reset using the GPS noted above, usually at the beginning of a monthly observing season. The arrival times and the ADC counts are recorded on a hard disk of a notebook computer.

The event rate is 2 to 3 Hz. The trigger rates of the tubes of the camera are 40 k to 140 k Hz. Those of the three-inch tubes are 0.1 k to 4 kHz. These rates vary with the amount of background photons. In addition, the light from the padding lamps contributes to the triggers of the tubes when the lamps are used. The rate of accidental coincidence between these triggers is negligibly small. In the case of the BIGRAT, η Scorpii is outside the field of view of the camera when PSR B1706−44 is tracked.

In each observing run gain calibration of camera tubes are performed by illuminating with the LEDs.

2.3. Stereoscopic observation

The 3.8-m telescope and the BIGRAT are operated simultaneously in order to obtain better S/N. In the stereoscopic observation the two telescopes track the same source. In a few observing runs the two telescopes track slightly different directions to each other. These directions are a little different from the source direction. We refer to this mode as 'non-parallel mode'. In the non-parallel mode the 3.8-m telescope tracks west of the source in right ascension and the BIGRAT tracks east. The difference is typically around 0.5°. Since the directions from the two telescopes to a shower position are slightly different, the rate of the coincident events is higher in the non-parallel mode operation. 0.5° is chosen in order to compensate for the difference of directions to a shower position. In fact the difference is about 0.7° in the case of a vertical shower whose center is at 8 km above. Trigger signals from the two telescopes are sent to each other during the observation. If two trigger signals are coincident in the time window of about 4 μs, the event is flagged as a coincident event for both telescopes.

The periods of stereoscopic observations described in this dissertation are listed in Table 3. The observation periods listed in Table 3 are a subset of the

Table 3 The periods of stereoscopic observation

Source	Month	Time of observation (hours)
PSR B1706−44	1994 May	6.7
	1995 May-Jul.	8.1*

*Observation in the non-parallel mode for 4.2 hours are included.

observation periods listed in Table 1.

3. Analysis

3.1. Data from the 3.8-m telescope

The analysis of image data obtained with the 3.8-m telescope is carried out in three steps, that is, the reduction of background photons in each image, image parameterization and event selection using the image parameters. After such analyses have been done, the number of the selected events from the on-source data and that from the off-source data have been compared in order to find out the flux of γ-rays from a point source.

Before the analysis of raw data, pedestal levels of ADC and TDC as well as the gain of each tube have been adjusted using the calibration data taken just before the run. The direction of the source in the field of view is calibrated using the images of stars. The image is indicated by high-rate signals from the tube on which the image is focused. The accuracy of the calibration is better than 0.02°.

Raw shower images contain not only Cherenkov photons but also background photons such as starlight and airglow. These backgrounds affect image parameters introduced below. Therefore, it is necessary to reduce backgrounds in images before the parameterization.

If the pulse height from a tube does not exceed the threshold value which corresponds to three or four photoelectrons, the signal from the tube is ignored.

Cherenkov photons arrive within the period of 10 ns, whereas the background photons arrive continuously. Thus, Cherenkov photons are discriminated from backgrounds using information of TDC. All the pulses which arrive within the period of $-37.5\ \text{ns} < t < 50\ \text{ns}$ are adopted, where t is the relative arrival times of pulses to the average arrival time of all pulses which arrive within 25 ns around a tentative origin which agrees roughly with the time which corresponds to the peak in the histogram of TDC counts. Events of which the number of tubes with pulses higher than the threshold is less than five are eliminated.

Cherenkov photons tend to cluster in a limited region in the field of view, whereas background photons distribute uniformly. Since background photons are usually isolated, any pulse without other pulses within the closest 24 tubes is ignored. This process is illustrated in Figure 10. In addition, if the sum of charges of all accepted pulses corresponds to less than 2.5 photoelectrons, the event is eliminated since it is likely to be a false event formed by electrical noise.

After the reduction of background photons mentioned above several parameters of the data obtained by the telescope are calculated (Figure 11). The axis of image is defined as a line which minimizes the charge-weighted sum of the square of the distances between the tubes with signals and the line. The axis roughly agrees with the shower axis on the image plane since Cherenkov photons emitted near the shower axis. The *alpha*, the most important parameter, is the angle of the image axis to the straight line from the centroid of the image to the direction of the source

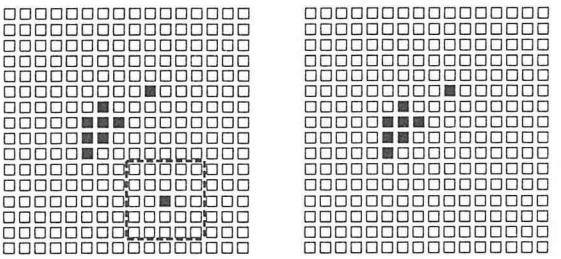

Fig. 10. Elimination of isolated signals from image data. Image data before (left) and after (right) elimination are shown. The filled squares represent the tubes with signals. The dashed line indicates a square including 5 tubes × 5 tubes. At the center of the square a tube with a signal is located. If there are no other tubes with signals in the square, the signal from the tube is ignored.

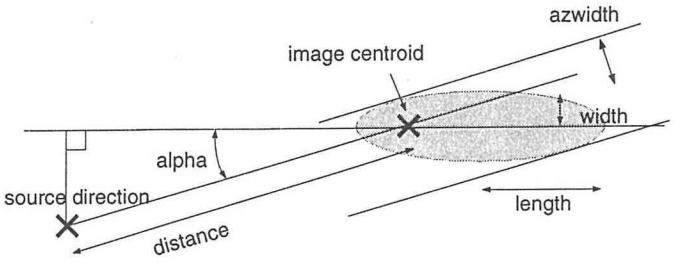

Fig. 11. A schematic view of the image parameters (see the text).

on the image plane. If the shower arrives from the source direction, the source direction is on the extension of the shower axis on the image plane. Thus, the image axis points toward the source direction on the image plane. As a result, *alpha* is close to zero in the case of γ-rays from the source. One the other hand, arrival directions of background cosmic rays are isotropic. Such events are scattered over the broad region of 0° to 90°. Using this difference γ-rays from the source are discriminated from cosmic rays.

The *length* and *width* are the standard deviations of the spreads of signals projected to the parallel and the perpendicular direction of the image axis respectively. The two parameters are related to vertical and lateral spreads of shower respectively. It has been found from simulations that *length* and *width* are likely to be larger in the case of hadrons than in the case of γ-rays. However, the difference is not as remarkable as that in *alpha*. These parameters are used mainly for eliminating false events in this work.

The *distance* is the length between the direction of the source and the centroid of the image on the image plane. Since the centroid of the image is the direction toward the shower position, *distance* is related to the arrival direction and the core location of the shower.

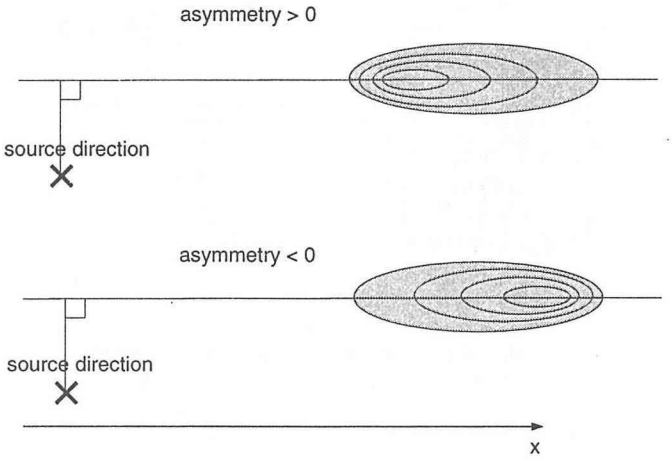

Fig. 12. A schematic view of the definition of *asymmetry*. When Cherenkov photons in the image are biased to the direction of the source on the image plane, *asymmetry* is positive. The x-axis shows the coordinate for the position of signal in the calculation of *asymmetry*.

The definitions of *length*, *width* and *distance* are the same ones as Hillas gave [22].

It is not always the case that whole the image collected in the reflector is observed with the camera. In order to eliminate such events, the parameter r_C is calculated, where r_C is defined as the distance between the centroid of the image and the center of the field of view. The r_C gives an estimation of the distance from the centroid of the image to the edge of the field of view. Since there are cases where the direction of the source on the image plane is different from the center of the field of view, r_C does not always agree with *distance*.

The *asymmetry* is the skewness of the spread of signals projected on the image axis. It is expressed as

$$asymmetry=\frac{1}{length}\left(\frac{\sum w_i (x_i-\bar{x})^3}{\sum w_i}\right)^{\frac{1}{3}},$$

where x_i is the position of the projection of the i-th tube with signal on the image axis, w_i is the charge of the signal and $\bar{x}$ is the charge-weighted average value of the positions. The position of the tube with signal is defined so as to increase with the distance from the source direction on the image plane to the projection as shown in Figure 12. This definition means that the image has positive *asymmetry* when the signals are biased to the source direction on the image plane. It is found from simulations that if a shower arrives from the direction of the source, *asymmetry* of the image of the shower is likely positive. Therefore, *asymmetry* is helpful to improve the angular resolution of the arrival direction of the shower.

The *azwidth* (AZimuthal WIDTH) is the standard deviation of the spread of signal projected on the perpendicular direction of the straight line which connects the direction of the source on the image plane and the the centroid of the image. The selection using *azwidth* improves the angular resolution for primary particles.

The arrival direction of the primary particle is close to the direction of the source in the case of the event with small *azwidth*. It is known that this parameter is more effective in the improvement of the angular resolution than *alpha* for image data obtained with a camera whose resolution is not so high. It is used in the analysis of image obtained with the BIGRAT.

The list of the cut with *alpha* and that with *asymmetry* as well as in previous observations is shown in Table 4. The objects from which significant signals have been obtained by the cut with *alpha* are limited. The results when *alpha* is used and those when *asymmetry* is also used are consistent for all the objects for which both of the parameters are used. It supports that the image analysis is a convincing method for detecting TeV γ-rays.

Events are selected by means of cuts using the parameters *alpha*, *length* , *width*, *distance*, r_C and *asymmetry*. The selection criteria are listed in Table 5. The criteria are chosen on the basis of simulations [26] for discrimination of the γ-ray events from background cosmic rays. The selection region on *alpha* is narrower in this work than that in the analysis for data in 1992-1993, where events with *alpha* less than 10° have been selected, since the accuracy of *alpha* decreases with the

Table 4. The list of the cut with *alpha* and that as well as *alpha* in previous observations. Other image parameters are also used for the cuts. The results have been given by the CANGAROO group except one observation of the Crab pulsar given by the Whipple group. "Yes" denotes that significant signals have been obtaind. "No" denotes that significant signals have not been obtained. "—" denotes that the cuts have not been applied.

Object	*alpha*	*alpha* and *asymmetry*
Vela pulsar [5]	Yes	Yes
PSR B1706−44 [3]	Yes	—
Crab pulsar [4]	Yes	—
PKS 0521−365 [23]	No	No
PKS 2005−489 [23]	No	—
W28 [24]	No	—
Crab pulsar (Whipple) [25]	Yes	Yes

Table 5. The criteria of the cut in the analysis of image obtained with the 3.8-m telescope. The *length*, *width*, *distance* and r_C are shown as angle.

alpha	$<5°$
length	$<0.4°$
width	$<0.3°$
distance	$>0.4°$
r_C+*length*	$<1.5°$
asymmetry	$>0°$

reflectivity of the reflector. The criteria of *width* and *length* are chosen so that an event is passed if it is not a false one which arises from noise. Since it is difficult to determine *alpha* of most images with small *distance*, events with *distance* less than 0.4° are eliminated. Most of an image is included in the circle with the radius of *length* whose center is located at the centroid of the image. Therefore, most of the image is observed if r_C+*length* is smaller than the radius of the field of view, which is about 1.5°. It is found from simulations that about 3/4 of images of γ-rays after the cut by *alpha*, *width*, *length*, *distance* and r_C have positive *asymmetry* are selected.

Distributions of *distance*, *width*, *length*, and *asymmetry* of the image data obtained in an on-source run and the corresponding off-source run are shown in Figure 13. The distributions in on-source run and off-source run are found to be almost the same.

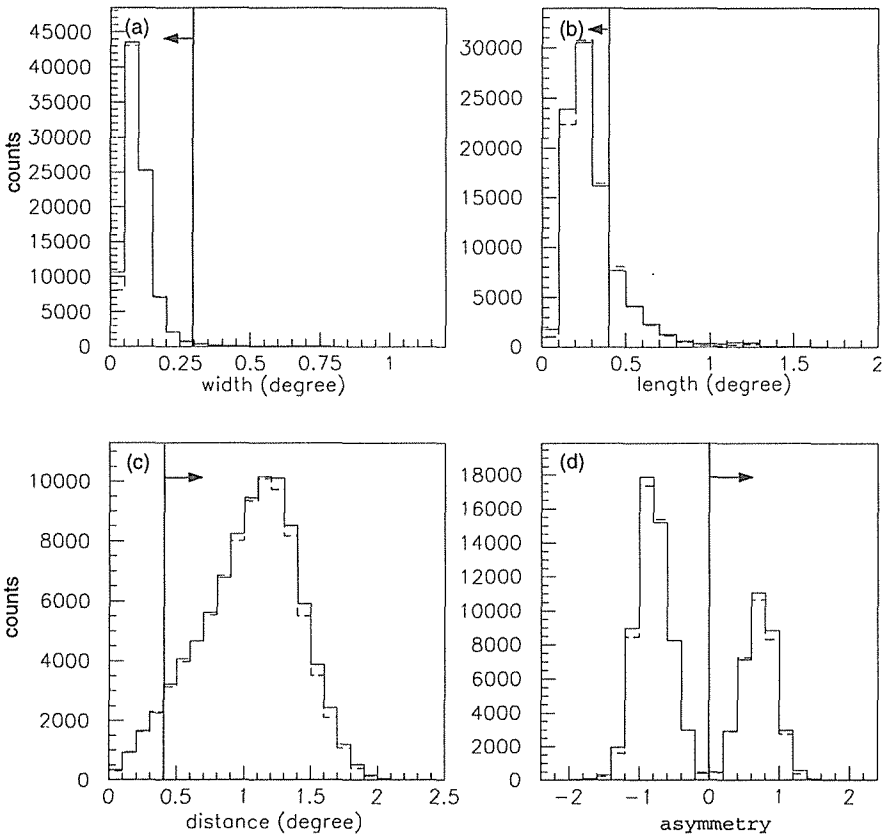

Fig. 13. The distributions of (a) *width*, (b) *length*, (c) *distance* and (d) *asymmetry* of image data obtained using the 3.8-m telescope for on-source (solid lines) runs and corresponding off-source (dashed lines) runs. The cuts by the image parameters have not been applied. The arrows indicate the selection criteria.

3.2. the BIGRAT data

The analysis of the BIGRAT data proceeds in four steps, that is, software padding, noise reduction, image parameterization and event selection. Software padding is applied only to the data observed in 1994 but are not applied to those in 1995 since the hardware padding was available in 1995.

The pedestal of ADC and the fluctuation of background photons are obtained from the data of the run. The pedestal level is determined from the distribution of ADC counts of the tube in two stages. At the first stage, the tentative ADC pedestal and standard deviation from it are determined using all events. At the second stage, only the events in which the tube does not detect 'signal' nor is adjacent to tubes with 'signals' are used for the calculation of the ADC pedestals. The 'signal' means that the ADC count is four times as large as the tentative standard deviation or more after subtracting the tentative pedestal. The fluctuation of the number of background photons for each tube is obtained by fitting the lower half of a Gaussian distribution to the histogram of ADC counts below the pedestal. The gain of each tube is calculated using the LEDs.

The noise level depends upon the location on the celestial sphere. This fact causes differences in the distributions of the image parameters between an on-source run and the corresponding off-source one. In the case of observation of PSR B1706−44, the noise fluctuation in off-source region is usually smaller than that in the on-source region. To compensate for the difference, artificial noise fluctuations are added to the signals from the tubes of off-source events using random numbers. The amount of fluctuation is calculated from noise fluctuations of the on-source data and the off-source ones. As a result the difference in the distributions of the image parameters between on-source runs and off-source ones disappears.

The next step is the reduction of background photons in image data. If the signal from a tube corresponds less than one photoelectron or the sum of the pulse

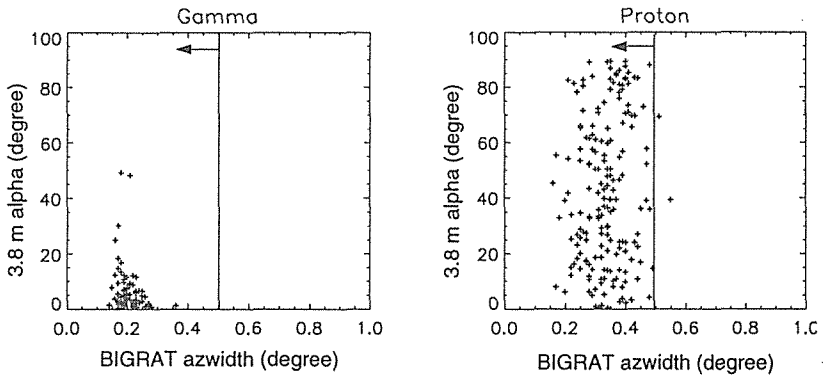

Fig. 14. Simulations on the correlation of *azwidth* of the BIGRAT and *alpha* of the 3.8-m telescope in the case of γ-ray events and in the case of proton events. The arrows show the selection region in the analysis (see the text).

height of the signals from the tube and the adjacent tubes to it corresponds to less than five photoelectrons, the signal from the tube is ignored.

The centroid of the image and *azwidth* are calculated for each coincident event with the 3.8-m telescope. The definition of *azwidth* has been given in Section 3.1. Monte Carlo simulations have revealed that *azwidth* is a better parameter than *alpha* to discriminate γ-ray events from hadron events in the case of the BIGRAT [27]. The centroid of the image is used in the stereoscopic analysis.

The events with *azwidth* smaller than 0.5° are selected. The simulations on *azwidth* for γ-rays and protons are shown in Figure 14. The surface of the reflector has been assumed to be an ideal parabola in the simulations. In consideration of the actual point spread function of the reflector, the selection region in the analysis is wider than the region expected from the simulations.

3.3. Stereoscopic analysis

As described in Section 1.3.3, combination of the shower images with the two detectors improves the signal-to-noise ratio. This improvement is made as the result of the coincidence of the events which are selected in the the analyses of both data from the 3.8-m telescope and the BIGRAT. It is confirmed by simulations that the combination of the criteria for image data observed with the 3.8-m telescope and those for BIGRAT data is helpful to eliminate proton events which are not eliminated in the analysis using only image data observed with a single telescope without eliminating γ-ray events (Figure 14). In the simulations the directions of primary γ-rays are vertical. Those of primary protons are randomly distributed within 3° around the vertical direction. The energies of the primary γ-rays and the protons follow the power-law with the index of -2.7. Only the events which are detected with both telescopes and pass the criteria of the analysis applied for image obtained with the 3.8-m telescope in the simulations are plotted in the figure. It is shown that there exist proton events whose *alpha* observed at the 3.8-m telescope is smaller than 5°. It is impossible to eliminate the events only using image at the 3.8-m telescope. However, a fair part of the events is eliminated without any loss of γ-ray events in the selection using *azwidth* at the BIGRAT. On the other hand, it is possible that proton events which are not eliminated with *azwidth* at BIGRAT are eliminated without any loss of γ-ray events using *alpha* at the 3.8-m telescope.

We can calculate the directions of the Cherenkov light from the information on the centroids of the shower images on the 3.8-m telescope and on the BIGRAT. The angle between the two directions deduced from the centroids on the both telescopes can be expressed with two parameters, θ_L and θ_T, where θ_L is the projection of the angle on the plane Π which is defined by the positions of both telescopes and the direction of the trajectory of the Cherenkov light deduced from the centroid of the image on the 3.8-m telescope as shown in Figure 15. θ_T is the projection perpendicular to this plane. The lengths of two trajectories of the Cherenkov light which correspond to two centroids of images on the 3.8-m telescope and the BIGRAT are referred to as l_A and l_B respectively. If the trajectories intersect each other, they are in the plane Π. In this case θ_T is zero. In the case

that $l \approx l' \gg d$, θ_L should be approximately d/l, where d is the distance between the two telescopes and l and l' are the distances between the telescopes and the intersection.

If an image in the telescope is highly deformed due to noise, the characteristics of the EAS is not reflected in the image parameters correctly. These events should be rejected. If *width*, *length*, *distance*, r_C+*length* or *asymmetry* of the image observed with the 3.8-m telescope or *azwidth* of the image observed with the BIGRAT is much different from the correct value, the event is eliminated by the criteria of these parameters. Stereoscopic analysis eliminates such events more severely. If the centroid of the image observed with one telescope is much different from the correct position due to noise, θ_T is much different from zero. If θ_T of an event is largely different from zero, the image is likely to be noise dominated. If the angular distribution of Cherenkov light is much different locally at one telescope from that at other locations, the characteristics of whole the EAS are not reflected by the image obtained with the telescope. It is likely that θ_T of such an event is largely different from zero. In order to eliminate these two types of events, the coincident events which satisfy $|\theta_T| < 0.4^\circ$ are selected. The width of the region is chosen to cover about 90% of coincident events.

The average θ_L in the case of non-parallel mode observation has been found to be larger than that in the case of parallel mode observation by about 0.1°. It means that the average heights where detected Cherenkov photons are emitted are low. This effect can be understood geometrically. The fields of view of the telescopes define cones along the optical axes. The overlapping region of the cones of the two telescopes is lower in the case of non-parallel mode observation. Thus, showers with lower emission region are more likely detected coincidently with the both telescopes. The average θ_T in the non-parallel mode observation is almost the same as in the parallel mode observation.

The distribution of θ_L and θ_T for the coincident events with the criteria of these parameters are shown in Figure 16. The distribution of θ_L is wider than that of θ_T. The main reason for this is the fact that the difference of θ_L is made also by the difference of the heights of the shower maxima.

It is possible to estimate the height of the shower maximum and the impact parameter at that point from θ_T and θ_T as follows. If the two trajectories of Cherenkov light l_A and l_B intersect each other, the intersection is the shower center. Since in fact the trajectories do not intersect, the intersection of l_A and l'_B, denoted as P in Figure 15, instead of that of l_A and l_B is calculated, where l'_B is the projection of l_B onto plane Π. The direction of this intersection agrees with the direction deduced from the image centroid at the 3.8-m telescope, whereas the direction of the intersection is $|\theta_T|$ apart from the direction deduced from the image centroid at the BIGRAT. Therefore, the point is used as the shower center. In order to compensate for the difference between the two telescopes, the intersection P is rotated by an angle of $\frac{|\theta_T|}{2}$ around the 3.8-m telescope perpendicularly to plane Π toward the direction shown in Figure 15. The direction of this point is $\frac{|\theta_T|}{2}$ apart from the direction deduced from the centroid of the image at the 3.8-m telescope and

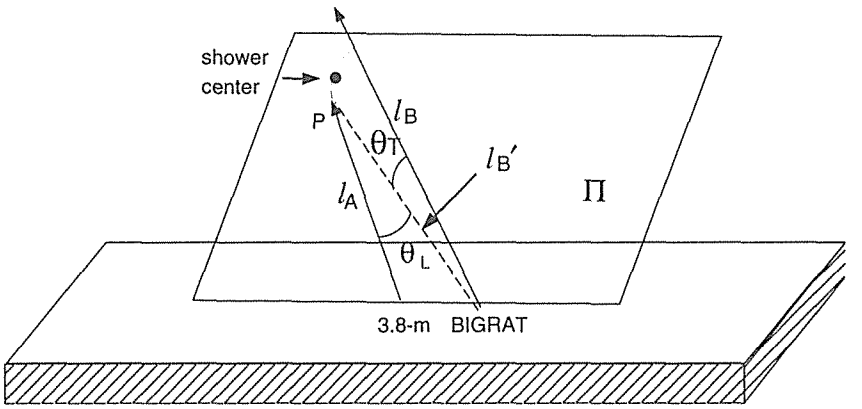

Fig. 15. The definitions of θ_L and θ_T. A plane(Π) is defined by the positions of the 3.8-m telescope and the BIGRAT and the direction of the centroid of the image observed with the 3.8-m telescope (l_A). In general, the trajectory of the Cherenkov light which corresponds to the centroid of the image observed with the BIGRAT (l_B) is not included on the plane. The dashed line indicates the projection of the trajectory on the plane(l_B'). P is the intersection of l_A and l_B'. The shower center is expected to be the point to which point P is rotated by $\frac{|\theta_T|}{2}$ around the 3.8-m telescope perpendicular to plane Π.

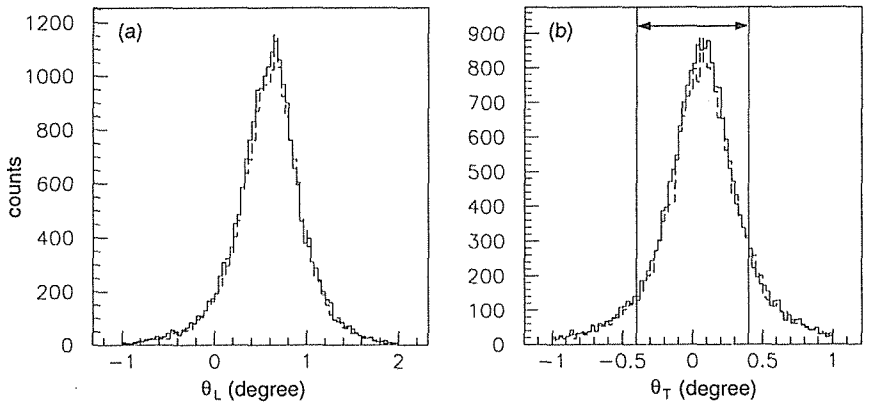

Fig. 16. Distributions of (a) θ_L and (b) θ_T for the coincident events of an on-source run (the solid line) and the corresponding off-source one (the dashed line). The arrow indicates the region in which the events are selected.

also an angle very close to $\frac{|\theta_T|}{2}$ apart from the direction deduced from the centroid of the image at the BIGRAT.

If we assumed that the primary particle arrives from the source direction, the core location of the shower on the ground is calculated from the shower center and the direction of the source.

3.4. Timing analysis

The arrival direction of each shower is not determined only from the shower image. However, the arrival direction is determined by combining the image and arrival times of Cherenkov photons contained in the image.

A plane is defined by the image axis as shown in Figure 17. The shower axis lies on the plane if we assume the image axis agrees with the shower axis on the image plane. The shower axis on the plane is represented by the angle of the arrival direction (θ) and the position of the shower core (r). Our aim is determining these two parameters from the arrival times of Cherenkov photons at the telescope. For the sake of simplicity we assume that the velocity of an EAS is equal to the velocity of light in a vacuum and all the Cherenkov photons are emitted on the shower axis. In addition, the Cherenkov photons are not expected to be scattered or refracted before they arrive at the telescope. The velocity of Cherenkov light is determined from the refractive index of the atmosphere. In this case, the arrival time of each Cherenkov photon at the telescope is simply calculated

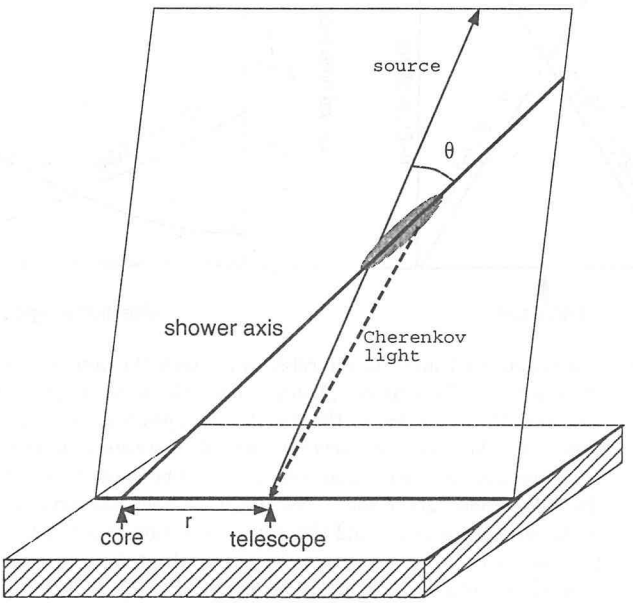

Fig. 17. The plane defined by the image axis is shown where *alpha* = 0. The shower axis lies on this plane. The angle (θ) between the shower axis and the source direction and the position of the core (r) are determined by fitting using the relation between the arrival times and the directions of detected Cherenkov photons.

as a function of the emitted position. The directions of detected Cherenkov photons at the telescope depend upon the emitted position. Therefore, the relation between the direction and the arrival time of a Cherenkov photon at the telescope is obtained as shown in Figure 18. Since the relation depends only on the arrival direction of the primary particle and the core location, it is possible to determine the both of them by measuring the direction and arrival time of Cherenkov photons

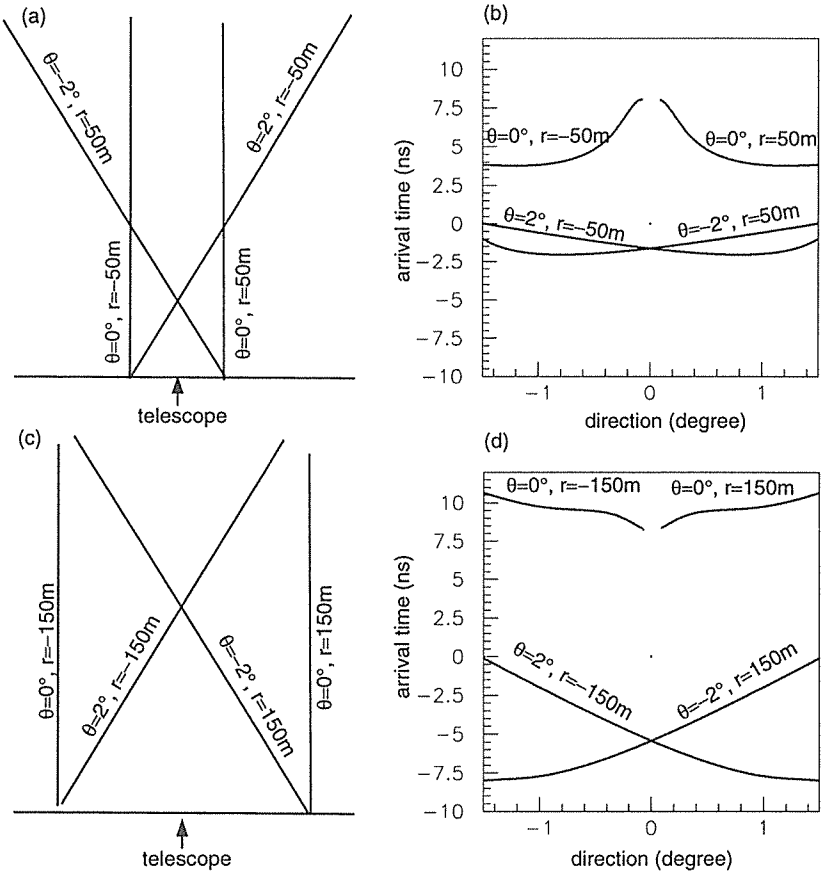

Fig. 18. The schematic feature of the relation between the arrival time and the direction of Cherenkov photons emitted from EASs when the direction of the source is the zenith and *alpha* = 0. Calculations are made for the cases of several arrival directions of the primary particles and the core distances. (a),(c) The shower axes for which the calculations are made. The angle between the arrival direction of the primary particle and the source direction is defined as θ. The position of the core is represented as r. The sign of r is defined so that when the sign of θ and that of r are the same, the shower axis does not intersect the line extended from the telescope toward the direction of the source. (b),(d) The arrival times of Cherenkov photons at the telescope as functions of the direction in the cases drawn in (a) and (c). The direction of Cherenkov photon is represented as an angle to the source direction. The origin of the arrival time is arbitrary.

simultaneously.

We determine the angle of arrival direction and the core location by two-parameter fitting (Figure 19). In the fitting the charge-weighted sum of the square of the difference between the arrival time of detected Cherenkov photon and that expected from the direction of the Cherenkov photon is minimized. Only relative arrival times among Cherenkov photons are measured in the observation. The average arrival time of all the detected Cherenkov photons of one event has been used as $t=0$ for fitting. The expected arrival time is calculated from the emitted point. Since Cherenkov photons are actually emitted off the shower axis with a certain angle, the emitted position of each Cherenkov photon is not determined uniquely from the direction of the Cherenkov photon. The closest point from the line which is extended from the telescope toward the direction of Cherenkov photon to the shower axis has been used as the emitted point. The line extended from the centroid of image to the source direction on the image plane has been used instead of the image axis for fitting for the sake of simplifying the calculation, because the two lines are almost the same, which means *alpha* is small, when the event is selected by the analysis of image data.

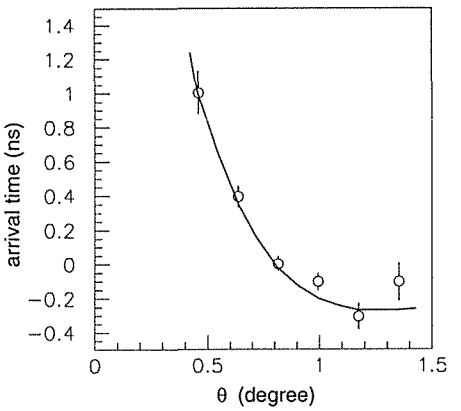

Fig. 19. A typical example of the correlation between the arrival time of Cherenkov photons and the angle to the source direction for a simulated event. Each circle represents the arrival time of the photons on one of the phototubes which corresponds to the angle θ to the source direction. The curve represents the fitted line from which the shower direction of the event is determined to 0.01° to the source direction.

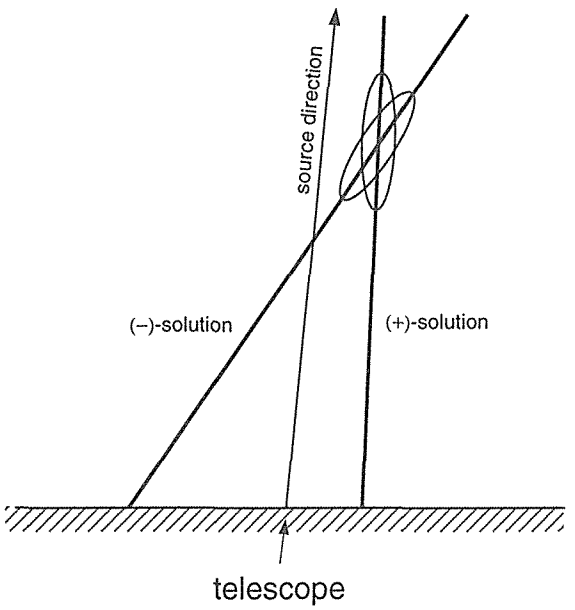

Fig. 20. A schematic explanation of two solutions in the fitting. In the case of (+)-solution, the centroid of the shower and the core position are located in the same side respect to the line extend from the telescope toward the source direction. In the case of (−)-solution, the shower centroid and the core position are located in the different sides.

In the execution of fitting, two solutions, one of which is a false one, are obtained in most cases. For one of the solutions the core and the centroid of shower are located in the same side respect to the line extended from the telescope toward the source direction, whereas for the other solution they are in the different sides (Figure 20). The solutions are referred to as (+)-solution and (−)-solution, respectively. The choice between two solutions has been made using *asymmetry*. From simulations it is found that if *asymmetry* is positive, the event has a (+)-solution in most cases, whereas if *asymmetry* is negative, the event has a (−)-solution in most cases.

Figure 21 shows the Monte Carlo simulation of the timing analysis. Reconstructed arrival directions of γ-rays from the point source are concentrated in the region close to zero. Such a concentration is not found in the case of protons. γ-ray events which have negative *asymmetry* form a bump around 2° since (−)-solutions are adopted for the events. However, the ratio of such events is about 1/4. Events for which fitting fails pile up at 4° because the region of arrival direction is limited within 4° in the fitting.

The arrival times and the directions of Cherenkov photons are measured with the 3.8-m telescope. The events with arrival direction from the source direction smaller than 1° are selected.

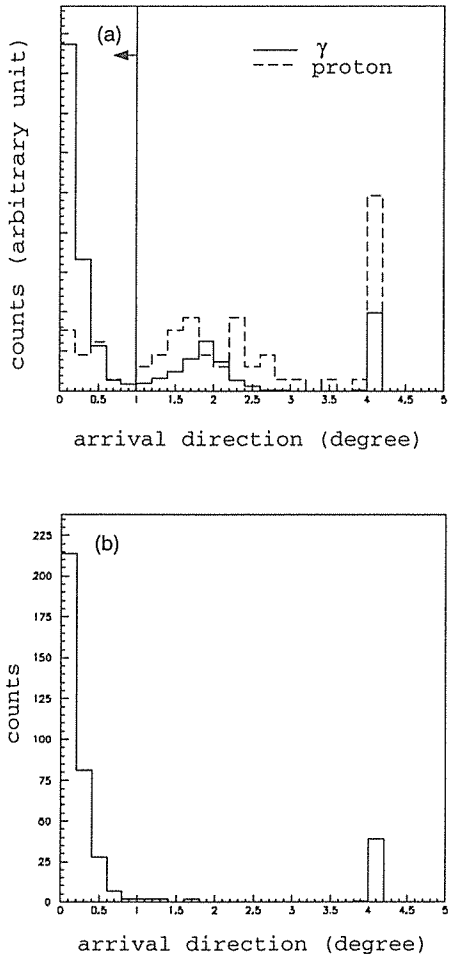

Fig. 21. (a) The arrival directions of primary particles ($|\theta|$) calculated from the images and the arrival times of Cherenkov photons generated by simulations. Events selected by analysis of image are observed at the 3.8-m telescope are plotted. The origin of the horizontal axis is the source direction. The solid line represents events from γ-rays and the dashed line represents ones from protons. Each scale has been chosen so that the number of γ-rays and the number of protons are equal. Events for which the fitting fails pile up at 4° because the region of arrival direction is limited within 4° in the fitting. The bump around 2° is formed by events which have negative *asymmetry*. The arrow indicates the region in the event selection. (b) γ-rays images of which have positive *asymmetry* are represented. The bump does not appear around 2°.

Table 6. The selection for PSR B1706−44 using the parameters of images obtained with the 3.8-m telescope. The criteria are listed in Table 5. The numbers of events before and after the selection are presented as total and selected respectively.

Year		N_{ON}	N_{OFF}	$N_{ON}-N_{OFF}$	Significance
1994	total	27895	28516	−621	—
	selected	388	333	55	2.0
1995	total	62515	59024	3491	—
	selected	692	595	97	2.7
1994+1995	total	90410	87540	2870	—
	selected	1080	928	152	3.4

4. Results

4.1. PSR B1706−44

4.1.1. Image data from the 3.8-m telescope

The results of the analysis of the image data obtained with the 3.8-m telescope are listed in Table 6. N_{ON} and N_{OFF} represent the numbers of events for the on-source runs and for the off-source runs respectively. There are large differences between N_{ON} and N_{OFF} before the selection using the image parameters mentioned in Section 3.1. The differences are much larger than statistical fluctuations of the number of events. The differences arise from the existence of false events formed by background photons and electrical noise which are not fluctuated statistically. Since the image parameters of these events do not satisfy the criteria listed in Table 5, the events are eliminated by means of the selection.

The numbers of events for PSR B1706−44 which are selected by the cut on the image observed with the 3.8-m telescope with criteria shown in Table 5 are listed in Table 7. The number of events which satisfies the criterion of *alpha* is the smallest. The number of events is reduced to about 1/20 by the cut. The criterion of *asymmetry* is the second severest. It reduces the number of events to

Table 7. The number of events for PSR B1706−44 selected by the cut on the image data observed with the 3.8-m telescope. The number of events before the cut is sown as 'total'.

Selection		N_{ON} (Radio to total)	N_{OFF} (Radio to total)
total		90410 (1.00)	87540 (1.00)
alpha	$< 5°$	4332 (0.05)	4061 (0.05)
width	$< 0.3°$	89502 (0.99)	86648 (0.99)
length	$< 0.4°$	72603 (0.80)	70654 (0.80)
distance	$> 0.4°$	85229 (0.94)	82369 (0.94)
r_C+*length*	$< 1.5°$	58679 (0.65)	58427 (0.67)
asymmetry	>0	34219 (0.38)	32774 (0.37)

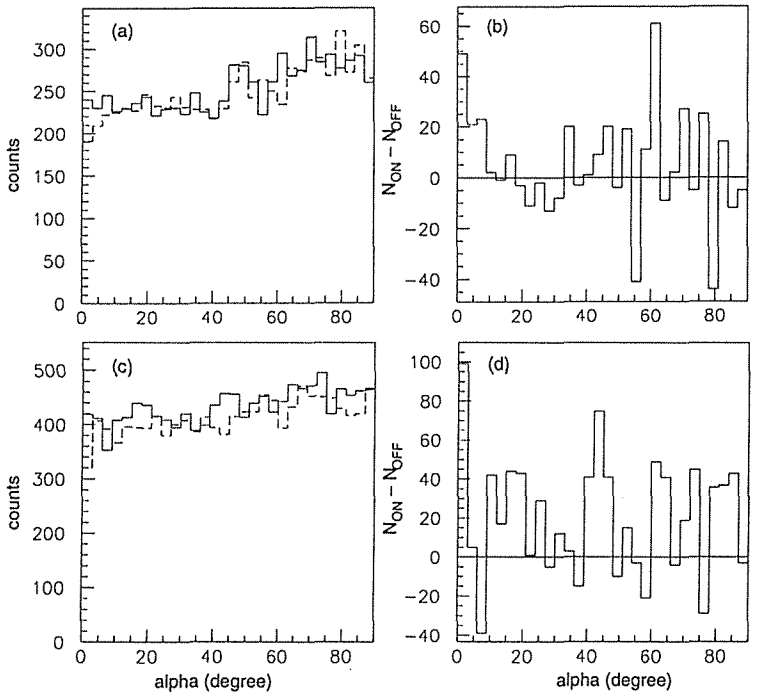

Fig. 22. The numbers of events from the direction of PSR B 1706−44 observed in 1994 and 1995 as a function of *alpha* after the event selection using *width*, *length*, *distance*, r_C and *asymmetry* in the analysis of images observed with the 3.8-m telescope are shown in (a) and (c) respectively. The solid lines indicate the distribution for on-source runs. The dashed ones indicate the distribution for off-source runs. The differences of the numbers of events between on-source runs and off-source runs in 1994 and in 1995 are shown in (b) and (d) respectively.

approximately 1/3.

After the selection the number, $N_{ON} - N_{OFF}$, in 1994 and 1995 is 152 in total. The statistical significances of these excesses are 3.4 σ, where σ is given by $\sqrt{N_{ON}+N_{OFF}}$. The numbers of events as a function of *alpha* after selection by the cut with *width*, *length*, *distance*, r_C and *asymmetry* are shown in Figure 22.

Threshold energy and flux The flux of TeV γ-rays from PSR B1706−44 is calculated using Monte Carlo simulations. The simulations have been carried out for the production of EASs initiated by γ-rays, the emission of the Cherenkov light from the EASs, the propagation of the light, the response of the 3.8-m telescope to the light and the analyses mentioned in Section 3.1. Airglow is added to image data as background photons. The energies of γ-rays are in the region of 0.5 to 10 TeV. The zenith angle from which the simulated γ-rays arrive is 20°, which agrees roughly with the average zenith angle for observation of PSR B1706−44. The locations of the cores are assumed to be distributed uniformly in a circle of 200 m in radius around the 3.8-m telescope. The threshold value of signal from each tube of the camera is three photoelectrons.

The integrated flux above the energy E is given by

$$\frac{N_\gamma}{TS}\left(\frac{E}{E_{min}}\right)^{n+1},$$

where N_γ is given as $N_{ON}-N_{OFF}$, T is the total period of observations, E_{min} is the minimum energy of γ-rays in the simulations and S is the collection area of γ-rays above E_{min} which is determined using the simulations. The n is the index of the power law. S is given as ηS_0, where η is ratio of the number of events which are triggered and selected in the analysis of the image data to the number of total events in the simulations, S_0 is assumed to be $200^2\pi\cos 20^\circ$ m^2. S depends on the energy spectrum of γ-rays. In these simulations, we assume that $E_{min}=0.5$ Tev.

The data observed by CANGAROO group in 1992 and 1993 is used in order to estimate the index n. The numbers of γ-ray events after selection by the cuts with image parameters are determined in three energy bands. The energy bands are below 2 TeV, 2 to 4.5 TeV and above 4.5 TeV. The energy of a γ-ray is estimated from the total charge of the signal from the camera. The number of γ-rays in each energy band is corrected using the collection area in the energy band. These collection areas are calculated as the same way as S. The corrected numbers of γ-rays have been fitted to a power law. The best fit of n has been found to be about -2.9.

In this case S has been calculated to be 3.3×10^7cm^2 in the simulations.

By assuming that $n=-2.9$ from 1992 and 1993 data, Monte Carlo calculation is done to estimate the threshold energy of detected γ-rays. The energy dependence of the spectrum produced in the simulations is shown in Figure 23. If the energy with the highest counting rate is regarded as the energy threshold for γ-rays, it is determined to be approximately 2 TeV.

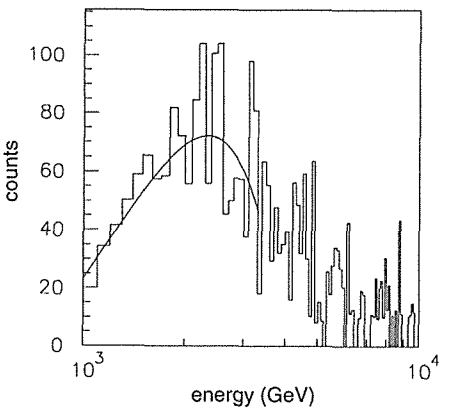

Fig. 23. The effective yield of the selected γ-rays versus energy of γ-rays produced by the Monte Carlo simulation. The energies of γ-rays follow the power-law with the index of -2.9. The zenith angle the direction from which the γ-rays arrive is 20°. The counting rate is found to be the highest around 2 TeV. The curve is obtained by fitting a Gaussian distribution.

The flux from PSR B1706−44 in 1994 and 1995 has been found to be $(1.3\pm 0.4)\times 10^{-11}\left(\frac{E}{\mathrm{TeV}}\right)^{-1.9}\mathrm{cm}^{-2}\mathrm{s}^{-1}$ above the energy E[†]. The calculated flux varies from $1.1\times 10^{-11}\left(\frac{E}{\mathrm{TeV}}\right)^{-1.7}\mathrm{cm}^{-2}\mathrm{s}^{-1}$ to $1.5\times 10^{-11}\left(\frac{E}{\mathrm{TeV}}\right)^{-2.1}\mathrm{cm}^{-2}\mathrm{s}^{-1}$ according as the index varies from −2.7 to −3.1.

If N_γ is much smaller than N_{CR}, which is the number of background cosmic rays, the significance of signals is given by

$$\frac{N_{ON}-N_{OFF}}{\sqrt{N_{ON}+N_{OFF}}}=\frac{N_\gamma}{\sqrt{2N_{CR}}}=\frac{fST}{\sqrt{2R_{CR}T}}=\left(\frac{\sqrt{2R_{CR}}}{S}\right)^{-1}f\sqrt{T},$$

where f is the flux of γ-rays and R_{CR} is the event rate of background cosmic rays. R_{CR} is calculated from the results of the analysis of off-source data. $\frac{\sqrt{2R_{CR}}}{S}$ represents the sensitivity of the telescope to γ-rays above E_{min}. It is independent of the flux and the time of observation. The sensitivity depends both on the apparatus and on the method of analysis. The sensitivity of the 3.8-m telescope has been calculated to be $3.0\times 10^{-10}\mathrm{cm}^{-2}\mathrm{s}^{-\frac{1}{2}}$ in the case that only image data has been used for the analysis. The sensitivity of the Whipple telescope is $9.9\times 10^{-10}\mathrm{cm}^{-2}\mathrm{s}^{-\frac{1}{2}}$ when 'super cut' is used. The 'super cut' is an analysis method developed on the basis of the observation of the Crab by the Whipple collaboration. When the image analysis is applied, the sensitivity of the 3.8-m telescope is better than that of the Whipple telescope, although the energy threshold of the Whipple telescope is lower.

4.1.2. Stereoscopic analysis

The results of the analysis for the events detected with the 3.8-m telescope and those of the events coincident with the BIGRAT are shown in Table 8. About half of the events detected with the 3.8-m telescope are coincident events. There are no large differences between N_γ/N_{CR} of the total events observed with the 3.8-m telescope and that of coincident events.

Table 8. The events from the direction of PSR B1706−44 detected in stereoscopic observations. The selection has been done by means of the parameters of images obtained with the 3.8-m telescope of "total" events and "coincident" events. The "total" in this table is the number of events obtained during the stereoscopic observation, which is included in the selected events in Table 5.

Year		N_{ON} (Ratio to total)	N_{OFF} (Ratio to total)	$N_{ON}-N_{OFF}$	$\frac{N_{ON}-N_{OFF}}{N_{OFF}}$
1994	total	293 (1.00)	218 (1.00)	75	0.34
	coincident	140 (0.48)	101 (0.46)	39	0.39
1995	total	325 (1.00)	258 (1.00)	67	0.26
	coincident	199 (0.61)	159 (0.62)	40	0.25
1994+1995	total	618 (1.00)	476 (1.00)	142	0.30
	coincident	339 (0.55)	260 (0.55)	79	0.30

[†]If the threshold value of signal from each tube of the camera is 3.5 photoelectrons, the calculated flux increases to $(1.7\pm 0.5)\times 10^{-11}\left(\frac{E}{\mathrm{TeV}}\right)^{-1.9}\mathrm{cm}^{-2}\mathrm{s}^{-1}$.

The events selected by the cuts on *azwidth* obtained from the BIGRAT data and θ_T obtained from the data on the two telescopes mentioned in Section 3.3 are shown in Table 9. It is shown that N_γ/N_{CR} can be improved by these selections from 0.30 to 0.37 and significance from 3.2 σ to 3.5 σ.

The sum of the events which have been selected by the stereoscopic analysis and the events which have been detected only with the 3.8-m telescope and selected by the image analysis is listed in Table 10. The significance is improved to 4.5 σ due to the increase in the number of events. The sensitivity is $1.6\times10^{-10}\mathrm{cm}^{-2}\mathrm{s}^{-\frac{1}{2}}$.

From these results it has been found that the stereoscopic analysis is an effective method to observe TeV γ-rays It is shown that even in the case that the angular resolution for the detection of Cherenkov lights with one of the telescopes is not so good, the stereoscopic analysis works effectively.

Table 9. The events from PSR B1706−44 selected by the cuts on *azwidth* of image in the BIGRAT and θ_T obtained from the data on the two telescopes mentioned in Section 3.3. The figures before the selection are shown as "3.8-m image". The results of the cut on θ_T are possibly improved also due to the statistical fluctuations of $N_{ON}-N_{OFF}$.

Year	Selection	N_{ON}	N_{OFF}	$N_{ON}-N_{OFF}$	$\frac{N_{ON}-N_{OFF}}{N_{OFF}}$	Significance
1994	3.8-m image	140	101	39	0.39	2.5
	azwidth	132	96	36	0.38	2.4
	θ_T	132	91	41	0.45	2.7
	azwidth and θ_T	124	87	37	0.43	2.5
1995	3.8-m image	199	159	40	0.25	2.1
	azwidth	186	147	39	0.27	2.1
	θ_T	180	136	44	0.32	2.5
	azwidth and θ_T	168	127	41	0.32	2.4
1994+1995	3.8-m image	339	260	79	0.30	3.2
	azwidth	318	243	75	0.31	3.2
	θ_T	312	227	85	0.37	3.7
	azwidth and θ_T	293	214	79	0.37	3.5

Table 10. Sum of the events obtained in the observation of PSR B1706−44. The summation has been done for the coincident events which have been selected by the stereoscopic analysis and events which have been selected by the stereoscopic analysis and events which have been detected only with the 3.8-m telescope and selected by the image analysis.

Year	N_{ON}	N_{OFF}	$N_{ON}-N_{OFF}$	$\frac{N_{ON}-N_{OFF}}{N_{OFF}}$	Significance
1994	277	204	73	0.36	3.5
1995	294	226	68	0.30	3.0
1994+1995	571	430	141	0.33	4.5

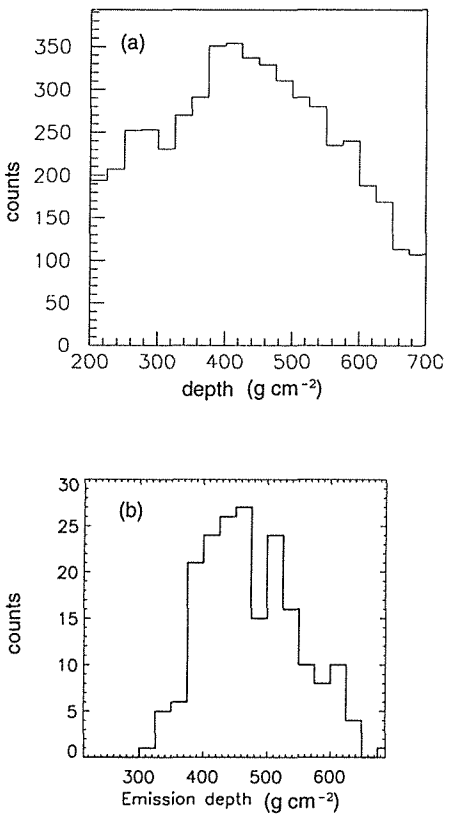

Fig. 24. (a) The number of off-source events as a function of the depth of shower centroid calculated by the stereoscopic analysis. These are coincident events obtained with the 3.8-m telescope and the BIGRAT in the observation of PSR B1706−44 in parallel mode. Any selection of imaging analysis on the data from the 3.8-m telescope is not made to the shown data. (b) The number of events as a function of average depth of Cherenkov photon emission obtained by the simulation. The Cherenkov photons detected with the 3.8-m telescope are used for the calculation of the average depth. Primary particles are assumed to be protons which arrive randomly from directions within 3° of the zenith. The spectral index of the protons has been assumed to be −2.65.

In Figure 24 are shown the number of events as a function of the depth of shower centroid calculated by the stereoscopic analysis, observed data in (a) and simulated one in (b). The depth of the mode in the observed events are fairly consistent with the one obtained by the simulations. The main reason for the wider spread in the observed events is ascribed to the errors of image centroids obtained with the two telescopes.

The numbers of events as a function of core location calculated from the images in the 3.8-m telescope and the BIGRAT are shown in Figure 25. The spread of locations shows the observed areas overlapped for both telescopes. However, the

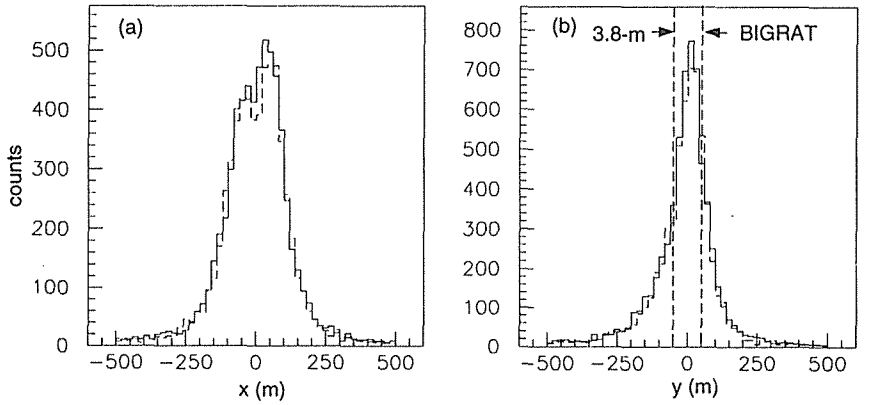

Fig. 25. (a) The number of events as a function of x-coordinate and (b) that of y-coordinate of the cores obtained by the stereoscopic analysis of PSR B 1706−44. The horizontal axis of (a) is the x-coordinate of core and that of (b) is the y-coordinate of core. The data for on-source run and the corresponding off-source one in parallel mode operation are indicated by the solid line and the dashed one, respectively. The origin of coordinates is the midpoint between the 3.8-m telescope and the BIGRAT. The 3.8-m telescope and the BIGRAT are located at the points (0, − 50 m) and (0, 50 m), respectively. The vertical dashed lines in (b) show the locations of the two telescopes.

spread should be slightly different from the real one since calculations have been made for the case where all showers arrive from the direction of the source.

4.1.3. Timing analysis

In Figure 26 are shown the number of events as a function of the arrival direction of the primary particle, where the events are selected by the analysis using the parameters of images observed with the 3.8-m telescope.

We can find some excess for $N_{ON}-N_{OFF}$ in the region where the arrival direction is close to the direction of the source. Smaller excesses are also found around 4° of the arrival direction. They are due to γ-rays for which we have failed in fitting as shown also in the simulations (Figure 21). The number of events as a function of *alpha* after the selection by using the arrival direction is shown in Figure 27. The excess where *alpha* is close to zero is significant compared to the one in the case of selection only with image data (Figure 22). Calculated arrival directions are physically meaningful only in the small-*alpha* region since small *alpha* is assumed in this calculation. These calculations have been performed in order to confirm that there are no systematic differences between on-source data and off-source data. Therefore, it it not necessarily true that the *alpha*-dependence of the event rate is flat near *alpha* equals zero in the case of off-source observation.

The results of selection by using the arrival direction of primary particle in addition to the image obtained with the 3.8-m telescope are listed in Table 11. The significance of $N_{ON}-N_{OFF}$ has been improved from 3.4 σ to 4.6 σ for the data in

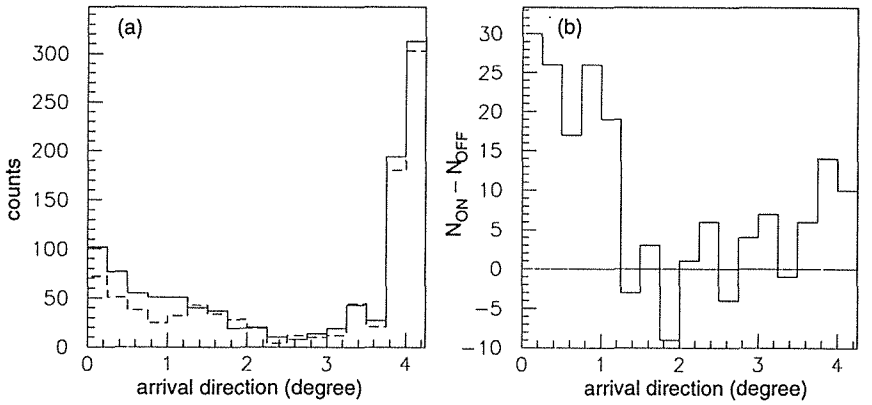

Fig. 26. (a) The number of events from the direction of PSR B1706−44 as a function of arrival direction selected by the analysis of image data from the 3.8-m telescope. The solid line indicates the number of events in on-source runs. The dashed one indicates the number of events in off-source runs. (b) The difference between the number of events in the on-source and that in the off-source runs.

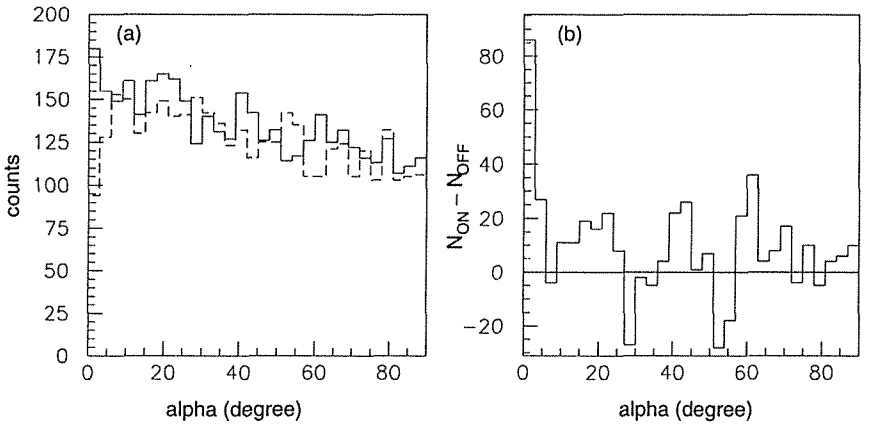

Fig. 27. (a) The number of events from the direction of PSR B1706−44 as a function of *alpha* after the selection by the timing analysis. The solid line indicates the distribution in the on-source runs. The dashed one indicates the distribution in the off-source runs. (b) The difference between the number of events in the on-source runs and that in the off-source runs.

Table 11. Events from the direction of PSR B1706−44 selected by using the arrival direction in addition to the selection by the image data analysis. The number of events selected only by the image data analysis is shown as "3.8-m image".

Year		N_{ON}	N_{OFF}	$N_{ON}-N_{OFF}$	$\frac{N_{ON}-N_{OFF}}{N_{OFF}}$	Significance
1994+1995	3.8-m image	1080	928	152	0.16	3.4
	selected	285	186	99	0.53	4.6

1994 and 1995. Therefore, the sensitivity has been improved from 3.0×10^{-10} $cm^{-2}s^{-\frac{1}{2}}$ to 2.1×10^{-10} $cm^{-2}s^{-\frac{1}{2}}$. These results show that the reconstructed arrival direction is helpful to select γ-ray events.

4.1.4. Combination of stereoscopic analysis and timing analysis

The results of the selection by the stereoscopic analysis and the timing analysis are listed in Table 12. The significance of $N_{ON}-N_{OFF}$ has been improved over the one obtained only by the stereoscopic analysis and the one obtained only by the timing analysis. It shows that the selection of γ-ray events in the two analyses is

Table 12. The results of combination of the stereoscopic analysis and the timing analysis for data of PSR B1706−44.

Year	N_{ON}	N_{OFF}	$N_{ON}-N_{OFF}$	$\frac{N_{ON}-N_{OFF}}{N_{OFF}}$	Significance
1994	72	40	32	0.80	3.0
1995	90	45	45	1.00	3.9
1994+1995	162	85	77	0.91	4.9

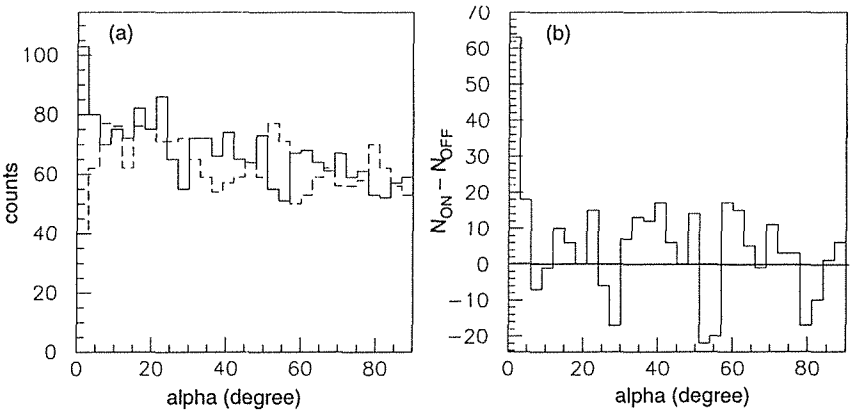

Fig. 28. (a) The number of events from the direction of PSR B1706−44 as a function of *alpha* after the the timing analysis is applied to the events listed in Table 10. The solid line indicates the distribution for on-source runs. The dashed one indicates the distribution for off-source runs. (b) The difference between the number of events in the on-source runs and that in the off-source runs.

not mutually exclusive, and that the elimination of background events is considerably independent. The number of events as a function of *alpha* after the selection is shown in Figure 28.

4.2. PSR B1055−52

The results of the selection mentioned in Section 3.1 are shown in Table 13. There is no significant difference between N_{ON} and N_{OFF} after the selection. Since it is found that the numbers of large-*alpha* events after the cut by *width*, *length*, *distance*, r_C and *asymmetry* are significantly different between on-source runs and off-source ones, N_{OFF} which has been normalized using the numbers of events with *alpha* larger than 30° are used in following results on PSR B1055−52. The numbers of events as a function of *alpha* after the selection are shown in Figure 29.

Table 13. The selection for PSR B1055−52 using the parameters of images obtained with the 3.8-m telescope. The criteria are listed in Table 5. The numbers of events before and after the selection are presented as total and selected respectively.

Year		N_{ON}	N_{OFF}	$N_{ON}-N_{OFF}$	Significance
1994	total	97037	103945	−6908	−
	selected	1234	1317	−83	−1.6
1995	total	43406	43930	−524	−
	selected	546	554	−8	−0.2
1994+1995	total	140443	147875	−7432	−
	selected	1780	1871	−91	−1.5

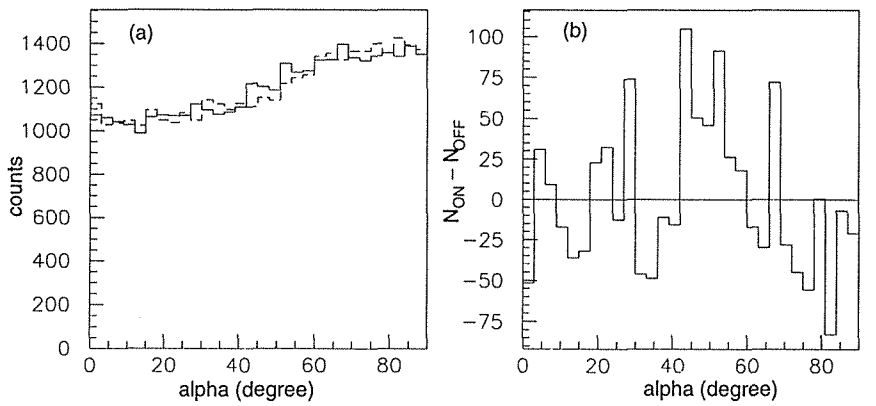

Fig. 29. (a) The number of events from the direction of PSR B1055−52 as a function of *alpha* after the event selection using *width*, *length*, *distance*, r_C and *asymmetry*. The solid line indicates the distribution for on-source runs and the dashed one indicates the distribution for off-source runs as a function of *alpha*. The numbers of events for off-source runs have been normalized using the numbers of events with *alpha* larger than 30°. (b) The difference of the number of events between on-source runs and off-source runs is shown.

Table 14. Events from the direction of PSR B1055−52 selected by using arrival direction in addition to the selection by the image data analysis. The number of events selected only by the image data analysis is shown as "3.8-m image".

Year		N_{ON}	N_{OFF}	$N_{ON}-N_{OFF}$	$\frac{N_{ON}-N_{OFF}}{N_{OFF}}$	Significance
1994+1995	3.8-m image	1780	1871	−91	−0.05	−1.5
	selected	507	579	−72	−0.12	−2.2

The upper limit of the flux from PSR B1055−52 has been calculated by the same simulations as in the case of the calculation for the flux from PSR B1706−44. The index has been assumed to be −2.7, which is a power-law index of background cosmic rays. The upper limit of the flux in 1994 and 1995 has been 1.5×10^{-12}cm^{-2}s^{-1} above 2 TeV at the 3 σ confidence level.

The results of selection by using the direction of primary particle in addition to the image analysis are listed in Table 14. There is no significant difference between N_{ON} and N_{OFF}. The upper limit of flux obtained by the timing analysis is lower than the one obtained by the analysis only with the image data obtained with the 3.8-m telescope. The upper limit of γ-ray flux from PSR B1055−52 has been calculated to be 9.5×10^{-13}cm^{-2}s^{-1} above 2 TeV at the 3 σ confidence level by the timing analysis. In this calculation it is assumed that the selection efficiency of the cuts of arrival direction for γ-rays from PSR B1055−52 is the same as in the case of PSR B1706−44. This upper limit is 0.64 times as high as the one in the case of the analysis only with the image data.

4.3. Centaurus A

The results of the selection mentioned in Section 3.1 are shown in Table 15. There is no significant difference between N_{ON} and N_{OFF} after the selection. The number of events as a function of *alpha* after the selection are shown in Figure 30. The upper limit of the flux has been calculated to be 2.6×10^{-12}cm^{-2}s^{-2} above 2 TeV at the 3 σ confidence level by the same simulations as in the case for the flux from PSR B1706−44. The index is assumed to be −2.7.

In this analysis we assume that the source of TeV γ-rays is a point-like one. It is inferred from observations of Cen A in the energy region of MeV to GeV that TeV γ-rays come from multiple sources or a diffused one around the direction of Cen A. If it is the case, the region of *alpha* of γ-ray events is broad. Accordingly,

Table 15. The selection for Cen A using the parameters of image obtained with the 3.8-m telescope. The criteria are listed in Table 5. The number of events before and after the 328-m telescope. The numbers of events before and after the selection are presented as total and selected respectively

Year		N_{ON}	N_{OFF}	$N_{ON}-N_{OFF}$	Significance
1995	total	198966	203071	−4105	−
	selected	2367	2334	33	0.5

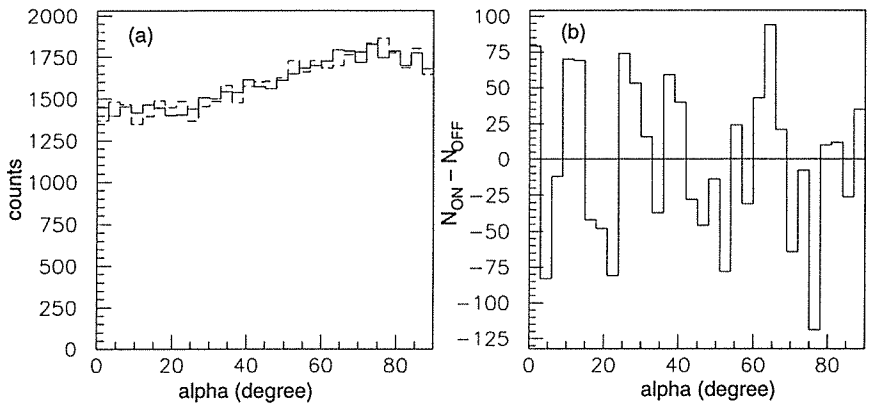

Fig. 30. (a) The number of events from the direction of Cen A as function of *alpha* after the event selection using *width*, *length*, *distance*, r_C and *asymmetry* has been done. The solid line indicates the distribution for on-source runs and the dashed one indicates the distribution for off-source runs. (b) The difference of the number of events between the on-source runs and the off-source runs is shown.

Table 16. Evets from the direction of Cen A selected by using arrival direction in addition to the selection by the image data analysis. The number of events selected only by the image data analysis is shown as "3.8-m image"

Year		N_{ON}	N_{OFF}	$N_{ON}-N_{OFF}$	$\frac{N_{ON}-N_{OFF}}{N_{OFF}}$	Significance
1995	3.8-m image	2367	2334	33	0.01	0.5
	selected	566	576	−10	−0.02	−0.3

the upper limit of the total flux from the multiple sources or the diffused source should be higher than the limit calculated above.

The results of selection by using the direction of primary particle in addition to the image analysis are listed in Table 16. There is no significant difference between N_{ON} and N_{OFF}. The upper limit of γ-rays flux from Cen A has been calculated to be $1.5\times10^{-12}\mathrm{cm}^{-2}\mathrm{s}^{-1}$ above 2 TeV at the 3 σ confidence level by the timing analysis. In this calculation it is assumed that the selection efficiency of the cuts of arrival direction for γ-rays from Cen A is the same as in the case of PSR B1706−44. This upper limit is 0.59 times as high as the one in the case of the analysis only with the image data.

4.4. Comparison of analysis methods

The performances of the analyses discussed above are summarized in Table 17. The significance of 4.6 σ and the S/N of 0.53 are obtained only using data from the 3.8-m telescope, whereas the significance of 4.9 σ and the S/N of 0.91 are obtained using data from the two telescopes.

Table 17. The comparison of the stereoscopic analysis and the timing analysis with analysis of image data from the 3.8m telescope.

Analysis	Data	$\frac{N_{ON}-N_{OFF}}{N_{OFF}}$	Significance	Sensitivity ($cm^{-2}s^{-\frac{1}{2}}$)
image	3.8-m	0.16	3.4	3.0×10^{-10}
stereoscopic	3.8-m+BIGRAT	0.37	3.5	2.1×10^{-10}
stereoscopic*	3.8-m+BIGRAT	0.33	4.5	1.6×10^{-10}
timing	3.8-m	0.53	4.6	2.1×10^{-10}
stereoscopic and timing	3.8-m+BIGRAT	0.91	4.9	1.3×10^{-10}

*when non-coincidence events are added.

5. Discussion

5.1. *Stability of TeV γ-ray emission from PSR B1706−44*

From the results of the analyses it is shown that PSR B1706−44 emitted γ-rays in 1994 and 1995. It is confirmed by using these results combined with the result obtained in 1992 and 1993 that PSR B1706−44 is a stable TeV γ-ray emitter. The fluxes in 1994 and 1995 are consistent with the fluxes in 1992 and 1993, assuming the index of the power law of the energy spectrum is −2.9 (Figure 31). The flux of TeV γ-rays is close to the extrapolated value of the energy spectrum from 1 to 10 GeV although γ-rays detected in the energy region between 50 MeV and 10 GeV are pulsed and γ-rays above 1 TeV detected in 1992 and 1993 are unpulsed. The significance of 3.4 σ obtained by the analysis of image data from the 3.8-m telescope is lower than that obtained from data in 1992 and 1993, that is, 12 σ. It is caused by shorter period of observation and possibly by lowering of reflectivity

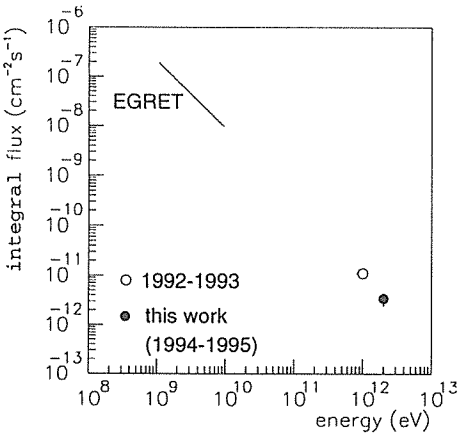

Fig. 31. The flux from PSR B1706−44. CANGAROO (1992-1993) data is cited from [28]. EGRET data is cited from [29].

of the mirror, although the possibility of a decrease in the flux is not completely excluded. The reflectivity in 1992 and 1993 is estimated about 55%, whereas that measured in 1994 and 1995 was about 40%. Simulations idicate that if the number of photons detected with the telescope reduces by 25%, the collection area decreases to roughly one half. This may be the reason for the decrease in significance.

5.2. Energy balance in PSR B1055−52

The upper limit of the flux above 2 TeV of PSR B1055−52 is 9.5×10^{-13}cm^{-2}s^{-1}. It is 10^{-5} times as large as the flux extrapolated from the spectrum in the energy region of 100 MeV to 4 GeV observed with EGRET as shown in Figure 32. The fact shows that there is a break in the spectrum in the energy region between 4 GeV and 2 TeV. Such a break is expected from the rotational energy of the pulsar since the luminosity of the pulsar exceeds the loss of the rotational energy unless the break exists. If the flux of PSR B1055−52 observed with EGRET extends above 4 GeV with the same power-law index, the upper limit of the cutoff energy is calculated to be 10 GeV from the constraint that the total luminosity does not exceed the rotational energy loss.

The upper limit of the luminosity of PSR B1055−52 above 2 TeV is calculated to be 1.2×10^{33}erg s^{-1} from the upper limit of the flux if the emission is isotropic. The luminosity of PSR B1055−52 as a function of energy is shown in Figure 33. The result in this work has revealed that the major components of the luminosity are γ-rays in the energy region of 100 MeV to 4 GeV and black body radiation in the energy region of X-rays. The latter is generally thought to be thermal radiation from the entire surface of the neutron star in initial cooling. The luminosity between 100 MeV and 5 GeV is $(9.4 \pm 1.6) \times 10^{33}$ erg s^{-1}. If there is a cutoff in the flux at 5 GeV, it is possible to expect that the remainder of rotational energy loss is

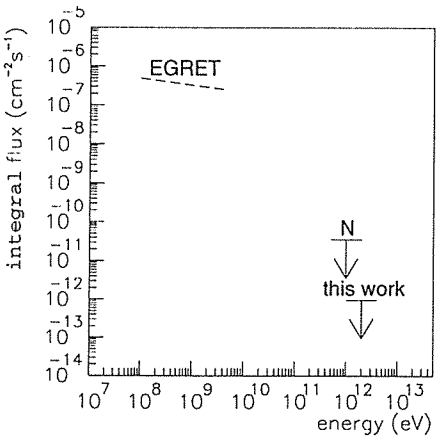

Fig. 32. The flux from PSR B1055−52. EGRET data is cited from [15]. The upper limit of pulsed TeV γ-rays(N) was measured at Nooitgedacht [30].

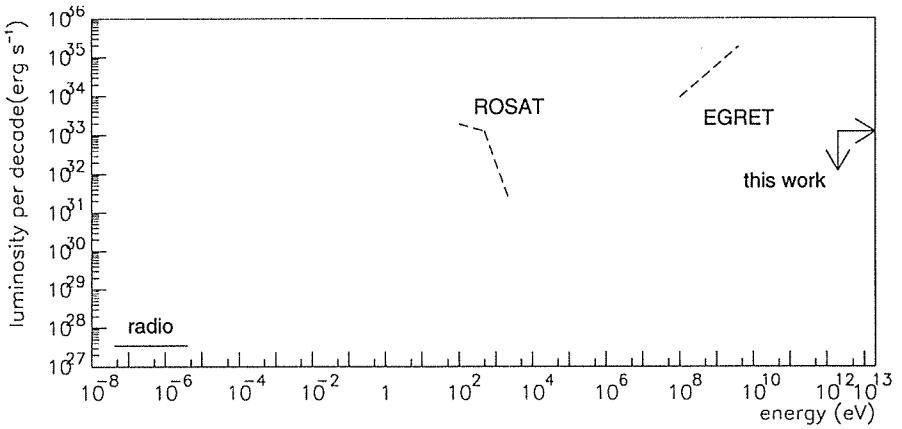

Fig. 33. The luminosity of PSR B1055−52 per decade of energy. The EGRET data is cited from [15]. ROSAT data and radio data are cited from [31] and [32] respectively.

converted to pulsar wind. In that case the energy flowing out as the pulsar wind is 2.1×10^{34} erg s^{-1}.

5.3. *Pulsar age and TeV γ-rays*

Observations of γ-rays in TeV region from five γ-ray pulsars including PSR B1055−52 have been done by several groups including the CANGAROO group. TeV γ-rays are detected from the three young pulsars among the five, namely PSR B1706−44, the Crab and the Vela pulsar have been detected. Since the two old pulsars, that is, PSR B1055−52 and Geminga are closer from the earth than PSR B1706−44 and the Crab, it is unlikely that the distances account for the trend. The trend is opposite in pulsed γ-rays in GeV region, where the efficiency of conversion from rotational energy of the pulsar to γ-rays increases with the age. It is generally accepted that energetic electrons in the pulsar nebula emit TeV γ-rays from the Crab by inverse Compton scattering. This views of the pulsar nebula responsible for TeV γ-rays are likely to explain also the case of the Vela and PSR B1706−44. For Geminga and PSR B1055−52, from which no TeV γ-ray emission has been detected, recent data from ROSAT and ASCA have implicated synchrotron X-ray nebulae around the objects. However, as Geminga is very close to the earth, namely, the distance is of the order of 100 pc, it may be difficult to observe TeV γ-rays from Geminga since the pulsar nebula is largely diffused. It is interesting to note that the Crab and the Vela pulsars are accompanied by SNRs and probably PSR B1706−44 also is, whereas PSR B1055−52 and Geminga are not. The fact suggests a possibility that the production of TeV γ-ray from a pulsar requires an SNR around it.

5.4. *Observations of Cen A in the energy region of TeV to PeV*

The upper limit of the flux above 2 TeV from Cen A obtained in this work is 1.5×10^{-12}cm^{-2}s^{-1}. In Figure 34 it is compared to previous observations in the

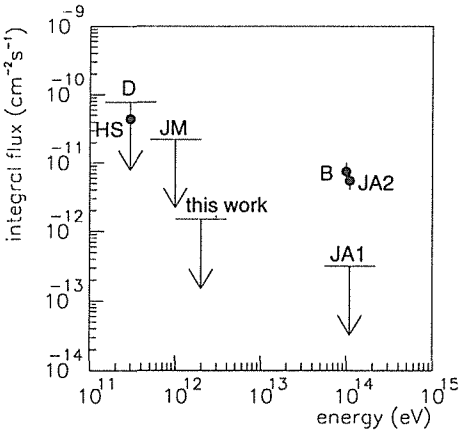

Fig. 34 The flux from Cen A in the energy region of TeV to PeV. Data are cited from [16](HS), [33](D), [34](JM), [35](JA1, JA2) and [36](B). The data in the energy region below 2 TeV have been obtained by Cherenkov-light telescope and the data in the energy region above 100 TeV have been obtained by air shower array.

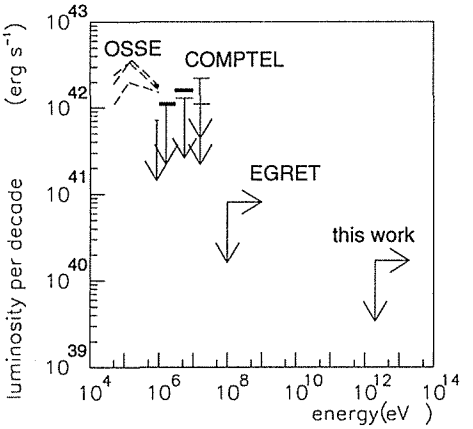

Fig. 35. The luminosity of Cen A as a function of energy. The data of OSSE, COMPTEL and EGRET are cited from [38], [17] and [39] respectively. It has been report that an unidentified source J1326−43 detected with EGRET might be Cen A.

energy region of TeV to PeV. It is not easy to understand all data consistently. One of the interpretations is that the flux from Cen A is variable in a time scale longer than a year as has been insisted up to now since these observations are not simultaneous. If it is the case, the result of this work means that Cen A was in quiet state in 1995. Indeed from 1992 at least to 1994 the flux from Cen A was smaller than that prior to the period in the energy region of keV to GeV [37] [38], although the relation between the flux below GeV and that above TeV is not obvious. However, in this case the variability by factor larger than 10 is necessary in the energy region above TeV. Another possibility is that γ-rays from Cen A are

contaminated by γ-rays from other sources within the angular resolutions of the detectors used for observations in which positive signals are detected. An unidentified source J1326−43, which has been detected with EGRET, might be one of such sources.

If we assume isotropic emission of TeV γ-rays from Cen A, the upper limit of the luminosity is 1.7×10^{40} erg s^{-1} above 2 TeV. The luminosity in the energy region of 50 keV to 1 MeV, which is the dominant contribution to the total luminosity (Figure 35), is 3.5 to 7×10^{42}erg s^{-1}. The luminosity fluctuates on a time scale longer than a year. Therefore, the luminosity in the energy region above 2 TeV is much smaller than that in the energy region of 50 keV to 1 MeV. This result shows that the total luminosity of Cen A obtained from the flux in the region of MeV is nearly correct.

5.5. TeV γ-ray emission from AGN

The upper limit of the flux above 2 TeV from Cen A is considerably low compared to the fluxes from Mrk 421 and Mrk 501. The fluxes from Mrk 421 above 0.5 TeV and from Mrk 501 above 0.3 TeV are 1.5×10^{-11}cm^{-2}s^{-1} and 8.0×10^{-12}cm^{-2}s^{-1} respectively. We assume that the power-law index of -2.7 for the spectra of γ-rays from these AGNs in order to normalize the observed fluxes with different energy threshold. Then, the upper limit of the luminosity of Cen A is 8.4×10^{-4} and 3.3×10^{-3} times as large as the luminosities of Mrk 421 and Mrk 501 respectively. TeV γ-rays from Mrk 421 and Mrk 501 might be absorbed in the intergalactic space, whereas the effect is negligible in the case of Cen A since it is much closer to the earth. Thus, the original luminosities of Mrk 421 and Mrk 501 are still higher. One of the possible explanations for high luminosities of Mrk 421 and Mrk 501 compared to that of Cen A is that the emissions of TeV γ-rays from Mrk 421 and Mrk 501 are concentrated in the direction of the jets. This explanation is reasonable if high energy γ-rays from AGNs are produced in the jets as is generally accepted. For example, in leptonic models the directions of the γ-rays are concentrated in the direction of the jet, since γ-rays are produced by inverse Compton scattering of relativistic electrons.

6. Conclusion

A search for TeV γ-rays from the pulsars PSR B1706−44 and PSR B1055−52 and from the radio galaxy Centaurus A were made with the two atmospheric Cherenkov telescopes of the CANGAROO collaboration, the 3.8-m telescope and the BIGRAT, at Woomera, Australia, in 1994 and 1995. The times of observations were 27 hours, 69 hours and 57 hours for these three sources, respectively. The 3.8-m telescope has a light-collecting reflector 3.8 m in diameter with a camera of 256 phototubes. The BIGRAT consists of three reflectors 4 m in diameter and a 37-phototube camera.

This dissertation has dealt with stereoscopic analysis and timing analysis applied to the CANGAROO data in addition to the imaging technique. The imaging

analysis has been applied only to the images of Cherenkov light detected with the 3.8-m telescope.

Two images simultaneously detected with the two telescopes have been utilized in the stereoscopic analysis, reducing the background events in which observed two images are not originated from one common shower. In the conventional imaging analysis, the extended structure of shower perpendicular to the line of sight is measured as an angular spread of image. On the other hand, the timing analysis provides us with new information on the direction of the primary γ-rays. The arrival time of Cherenkov photon on the detector depends upon the different path length of electrons and photons in the shower and the Cherenkov light. Thus, the timing analysis is a method of determining the arrival direction of shower with less ambiguity. The present work is the first one to report that such a timing analysis is found to improve the significance of γ-ray signal.

By the analysis of the data of the images on the 3.8-m telescope the sensitivity of the observation for PSR B1706−44 has been found to be $3.0 \times 10^{-10}\mathrm{cm}^{-2}\mathrm{s}^{-\frac{1}{2}}$ above 2 TeV. It has been improved to $2.1 \times 10^{-10}\mathrm{cm}^{-2}\mathrm{s}^{-\frac{1}{2}}$ by the stereoscopic analysis. Slightly better sensitivity can be obtained if events detected only with the 3.8-m telescope are added. The timing analysis is also helpful to improve the sensitivity. If the stereoscopic analysis and the timing analysis are combined in addition to the analysis of the image data on the 3.8-m telescope, the obtained sensitivity of the observation has been improved to $1.3 \times 10^{-10}\mathrm{cm}^{-2}\mathrm{s}^{-\frac{1}{2}}$. The ratio of the number of γ-rays from the source to the number of the cosmic ray background is 0.16 when only the analysis of the image on the 3.8-m telescope is applied. The ratio can be improved to 0.91 if the stereoscopic and timing analyses are also applied. We conclude that both of these two techniques are very useful for discriminating γ-rays from background cosmic rays in observation of TeV γ-rays.

The flux of TeV γ-rays from PSR B1706−44 observed in 1994 and 1995 has been found to be $(1.3 \pm 0.4) \times 10^{-11} \left(\frac{E}{\mathrm{TeV}}\right)^{-1.9}$ above the energy E. The energy threshold is approximately 2 TeV. This value is consistent with the previous observation in 1992 and 1993. Thus, PSR B1706−44 has been established as a stable TeV γ-ray emitter from the observation in 1992-1995.

There is no evidence of TeV γ-rays from PSR B1055−52 and Cen A. The upper limit of the flux above 2 TeV from PSR B1055−52 in 1994 and 1995 has been found to be $9.5 \times 10^{-13}\mathrm{cm}^{-2}\mathrm{s}^{-1}$ at the 3σ confidence level. The limit is 10^{-5} times as large as the value extrapolated from the spectrum in the region between 100 MeV and 4 GeV observed with EGRET. Thus, it is expected that a break in the spectrum between 4 GeV and 2 TeV. It is necessary that the cutoff energy is power than 10 GeV so that the total luminosity does not exceed the rotational energy loss of the neutron star. From results on the Crab pulsar, PSR B1706−44, the Vela pulsar, Geminga and PSR B1055−52, we can indicate a tendency that young γ-ray pulsars are likely to emit TeV γ-rays.

The upper limit of the flux above 2 TeV from Cen A in 1995 has been found to be $1.5 \times 10^{-12}\mathrm{cm}^{-2}\mathrm{s}^{-1}$ at the 3 σ confidence level. The flux is not consistent with the several previous results of detections of γ-rays from Cen A in the energy region

of TeV to PeV, unless either an increase in flux by a factor of 10 or more on a time scale of one year, or contamination of γ-rays from another source close to Cen A, is assumed to explain the reported results. The upper limit of the flux from Cen A corresponds to a luminosity of 1.7×10^{40}erg s^{-1} if isotropic emission is assumed. It is 8.4×10^{-4} and 3.3×10^{-3} times as large as the luminosities of Mrk 421 and Mrk 501 respectively.

In this work we have found that new techniques for detecting the EAS are of vital importance to observe new γ-ray sources in the energy region of 10 GeV to 10 TeV. The stereoscopic analysis will be one of the key techniques for future ground-based observations of γ-rays.

Several new Cherenkov-light telescopes with large reflectors and high resolution cameras are planned at present including the CANGAROO-II project. The energy threshold of the telescopes will be lower than the telescopes shown in this paper. The newly developed timing analysis will be helpful for improving the angular resolution in such telescopes for lower energy γ-rays, because it is based on elementary characteristics of the shower and Cherenkov light independent of the energy of primary particle. We believe that such new techniques developed in this work will contribute much to the future research of the high energy phenomena in the universe.

Appendix

Definitions of θ_L and θ_T

When the Cherenkov light from a cascade shower is observed with two telescopes, A and B, the elevation and the azimuth of the directions which correspond to the centroids of the shower images obtained by both telescopes are

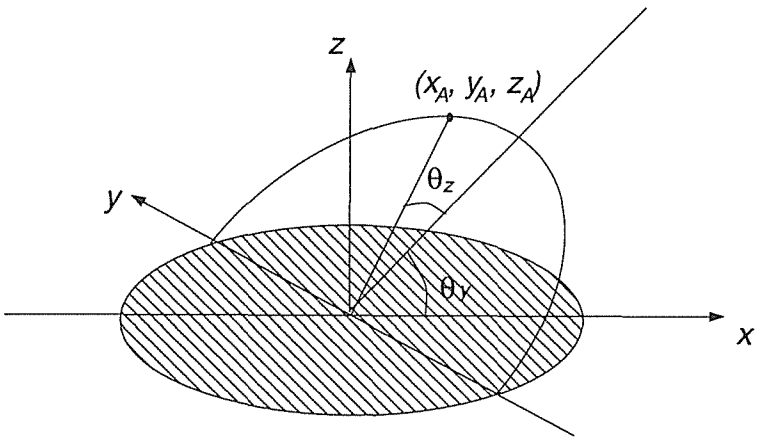

Fig. 36. Definitions of θ_y and θ_z (see the text).

defined as θ_A, θ_B and ϕ_A, ϕ_B, espectively. θ_L and θ_T satisfy the following relations:

$$\theta_L = -\arctan(y_B'/x_B'),$$
$$\theta_T = \arcsin z_B',$$

where (x_B', y_B', z_B') is defined to be the point to which (x_B, y_B, z_B) is rotated by $-\theta_z$ around the z-axis after rotated by $-\theta_y$ around the y-axis. θ_y is defined as the angle of the plane defined by the y-axis and (x_A, y_A, z_A) to the xy-plane and θ_z is defined as the angle of the straight line which connects the origin and the point to which (x_A, y_A, z_A) is rotated by $-\theta_y$ around the y-axis to the x-axis. (x_A, y_A, z_A) and (x_B, y_B, z_B) are defined to be the unit vectors which correspond to the two image centroids respectively. The ground corresponds to the xy-plane. The x-axis is the direction at which azimuth is zero. These are given by

$$\begin{pmatrix} x_{B'} \\ y_{B'} \\ z_{B'} \end{pmatrix} = \begin{pmatrix} \cos\theta_z & \sin\theta_z & 0 \\ -\sin\theta_z & \cos\theta_z & 0 \\ 0 & 0 & 1 \end{pmatrix} \begin{pmatrix} \cos\theta_y & 0 & -\sin\theta_y \\ 0 & 1 & 0 \\ \sin\theta_y & 0 & \cos\theta_y \end{pmatrix} \begin{pmatrix} x_B \\ y_B \\ z_B \end{pmatrix},$$

$$\theta_y = -\arctan(z_A/x_A),$$
$$\theta_z = \arcsin y_A,$$

$$\begin{pmatrix} x_A \\ y_A \\ z_A \end{pmatrix} = \begin{pmatrix} \cos\theta_A\cos\phi_A \\ \cos\theta_A\sin\phi_A \\ \sin\theta_A \end{pmatrix},$$

$$\begin{pmatrix} x_B \\ y_B \\ z_B \end{pmatrix} = \begin{pmatrix} \cos\theta_B\cos\phi_B \\ \cos\theta_B\sin\phi_B \\ \sin\theta_B \end{pmatrix}.$$

Acknowledgment

I would like to express my deep gratitude to all those who supported me to complete this work.

First, I would wish to thank my supervisor, Prof. A. Masaike, for helpful advice with tenacious encouragement from the beginning of the work to the completion of this dissertation. I address my thanks to Prof. T. Kifune and Prof. T. Tanimori for giving me an opportunity to begin this work and much advice on improving it. It is my pleasure to thank Prof. G. J. Thornton. It would be very difficult to carry out this work without his contributions, in particular, to the stereoscopic analysis. I thank Prof. K. Imai and Prof. H. En'yo for and giving comments since I entered this research field.

I also thank all the members of the CANGAROO group. I was much assisted by these members at Woomera in obtaining the data for this work.

Observations at Woomera were technically supported by Mr. N. Wild, the University of Adelaide.

I thank Prof. M. Matsuoka. He encouraged me when I was at the Institute of Physical and Chemical Research.

I am grateful to Ms. M. Hayashi, the Physics Department of Kyoto University, for her attentive assistance to this work in various aspects. Also to Ms. M. Masaike for her support when I was writing the manuscript in Kyoto.

It was fortunate that I was permitted to use a parallel computer in the Department of Physics, Tokyo Institute of Technology and computer resources in the Air Shower Division of Institute for Cosmic Ray Reserch, University of Tokyo. This made this work much easier.

A portion of this work was financially supported by Fellowships of the Japan Society for the Promotion of Science for Japanese Junior Scientists.

References

[1] T. C. Weekes, Ap. J., **342**, 379 (1989)
[2] G. Vacanti, Ap. J., **377**, 467 (1991)
[3] T. Kifune, et al., Ap. J. Lett., **438**, L91 (1995)
[4] T. Tanimori, et al., Ap. J. Lett., **429**, L61 (1994)
[5] T. Yoshikoshi, Detection of Very High Energy Gamma Rays from the Direction of the Vela Pulsar, PhD thesis, Tokyo Institute of Technology (1996)
[6] O. C. De Jager and A. K. Harding, Ap. J., **396**, 161 (1992)
[7] M. Punch, et al., Nature, **160**, 477 (1992)
[8] J. Quinn, et al., Ap. J. Lett., **456**, L83 (1996)
[9] F. W. Stecker, O. C. de Jager, and M. H. Salamon, Ap. J. Lett., **390**, L49 (1992)
[10] A. D. Kerrick, et al., Ap. J., **452**, 588 (1995)
[11] T. C. Weekes, Space. Sci. Rev., **59**, 315 (1992)
[12] P. J. Meintjies et al., Ap. J, **401**, 325 (1992)
[13] H. I. Nel, et al., Ap. J., **418**, 836 (1993)
[14] A. E. Vaughan, and M. I. Large., MNRAS, **156**, 27P (1972)
[15] J. M. Fierro, et al., Ap. J. Lett., **413**, L27 (1993)
[16] J. E. Grindlay, et al., Ap. J. Lett., **197**, L9 (1975)
[17] H. Steinle, et al., Adv. Space Res. **15**(5), 37 (1995)
[18] P. L. Nolan, et al., Ap. J. **459**, 100 (1996)
[19] P. M. Chadwick, et al., Space Sci. Rev., bf 75, 153
[20] A. Kohnle, et al., Astro. Part. Phys., **5**, 119 (1996)
[21] O. T. Tumer, et al., Proc. of 21st Interantioanl Cosmic Ray Conf. (Adelaide), **2**, 155 (1990)
[22] A. M. Hillas, Proc. of 19th International Cosmic Ray Conf. (La Jolla), **3**, 445 (1985)
[23] T. Ohsaki, M.Sc. thesis, Tokyo Institute of Technology (1996)
[24] M. Mori, et al., Proc. of 24th International Cosmic Ray Conf. (Roma), **2**, 487 (1995)
[25] M. Punch, New Techniques in TeV Gamma-ray Astronomy, Ph.D. thesis, National University of Ireland (1993)
[26] T. Tsukagoshi, M.Sc. thesis, Tokyo Institute of Technology (1994)
[27] G. P. Rowell, A search for Very High Energy Gamma Rays from PSR 1076−44 using the Atmospheric Cherenkov Imaging Technique, PhD thesis, University of Adelaide (1995)
[28] T. Tanimori, et al., Proc. of International Workshop 'Towards a Major Atmospheric Cherenkov Detector III'(Tokyo), 311 (1994)
[29] D. J. Thompson, et al., Ap. J., **465**, 385 (1996)
[30] H. I. Nel, et al., Ap. J., **398**, 602 (1992)

[31] H. Oegelman and J. P. Finley, Ap. J. Lett., **431**, L31 (1993)
[32] A. F. Cheng and D. J. Helfand, Ap. J., **271**, 271 (1983)
[33] A. Carraminana, et al., A&A, **228**, 327 (1990)
[34] W. H. Allen, et al., Ap. J., **405**, 554 (1993)
[35] W. H. Allen, et al., Astro. Part. phys., **1**, 269 (1993)
[36] R. W. Clay, et al., Astro. Part. phys., **2**, 347 (1994)
[37] I. A. Bond, et al., A&A, **307**, 708 (1996)
[38] R. L. Kinzer, et al., Ap. J., **449**, 105 (1995)
[39] C. E. Fichtel, et al., Ap. J., Supp., **94**, 551 (1994)